# *Constraining the Higgs-charm Yukawa coupling in the CMS experiment*

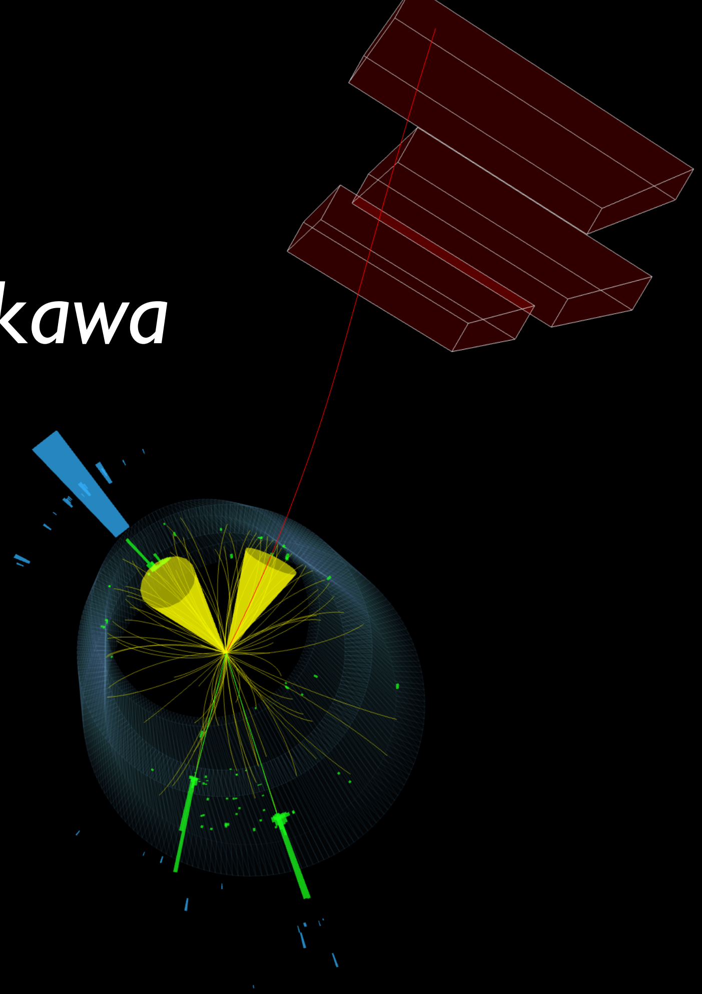

曲慧麟 (CERN)

中山–北大联合高能物理青年论坛
2022.05.18

# Introduction

❑ Discovery of the Higgs boson in 2012: A new chapter of particle physics

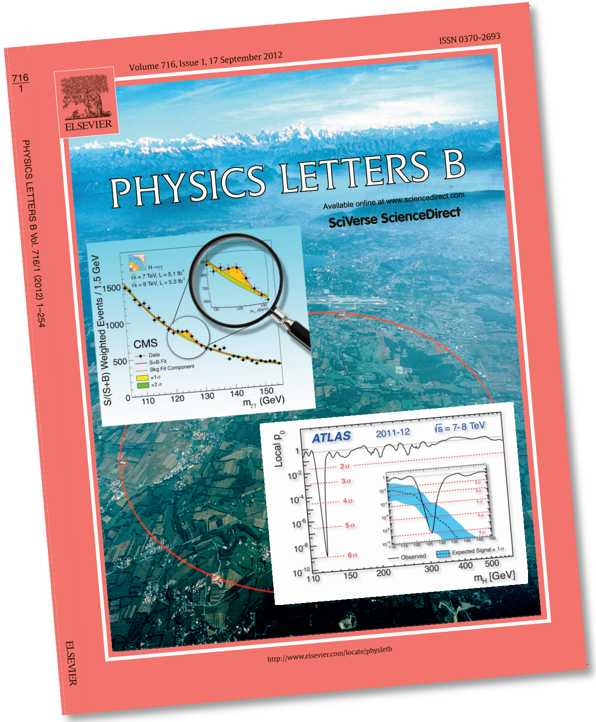


# Understanding the Higgs boson

- Tremendous progress in our understanding of the Higgs boson in the past ten years

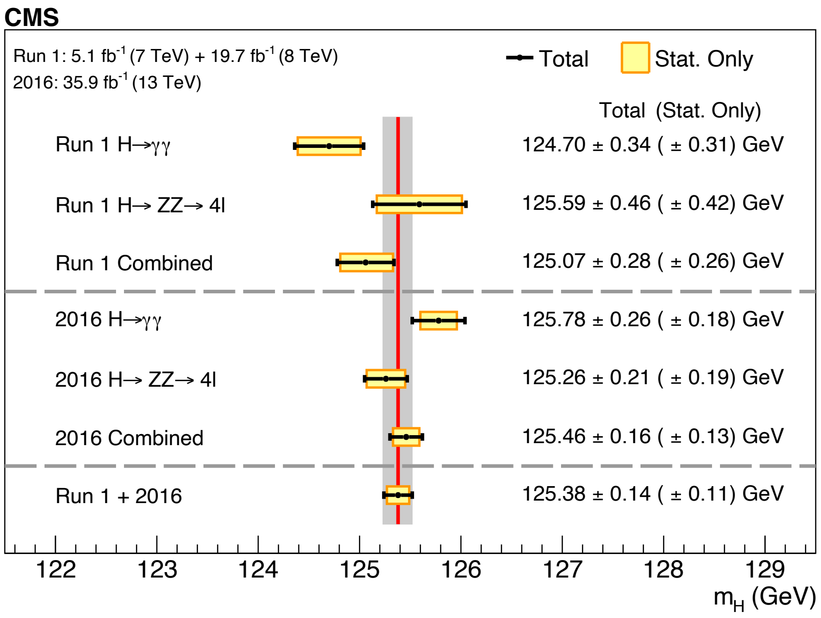


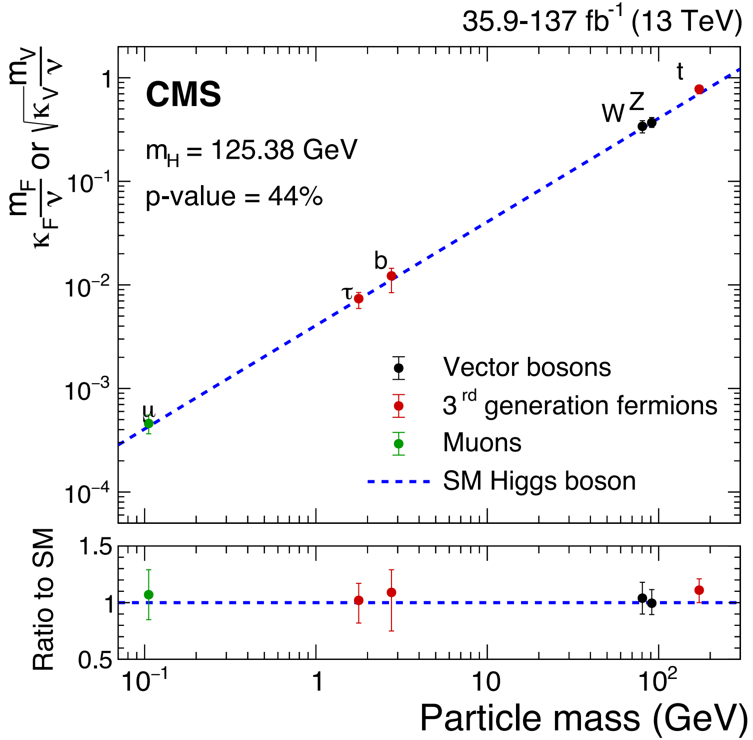

# How charming is the Higgs boson?

- Tremendous progress in our understanding of the Higgs boson in the past ten years

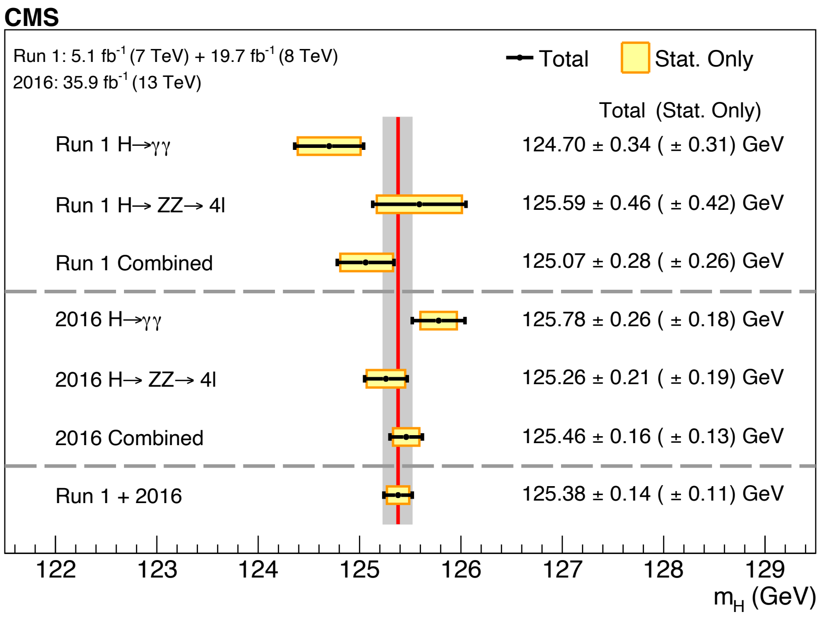


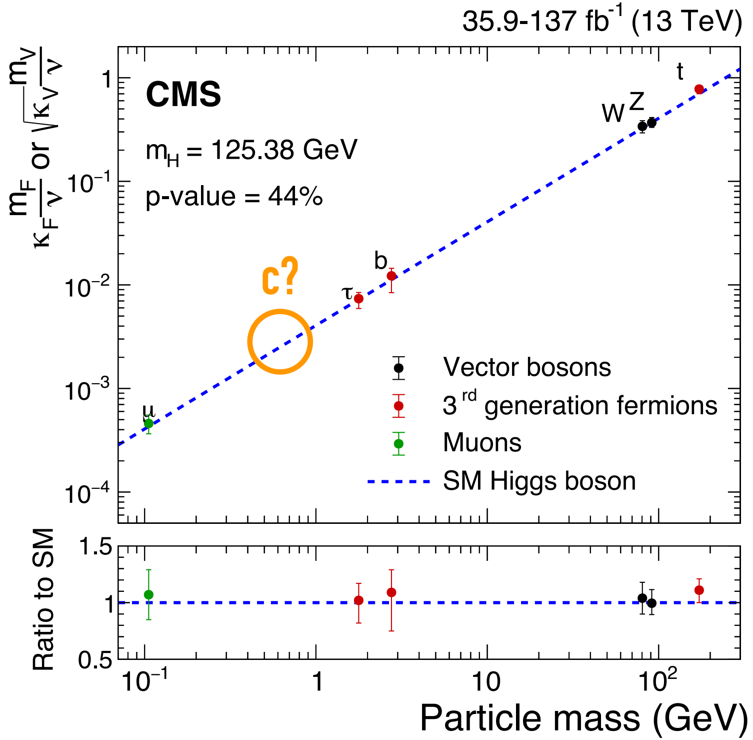

# Direct search for $H \to cc$

- Search for $H \to cc$ decays: directly sensitive to $y_c$, but very challenging
  - small branching fraction (~3%) vs. large backgrounds (at a hadron collider)
  - charm quark identification is the key
- Exploit associated VH production (V = W, Z)
  - three channels: $Z \to \nu\nu$ (0L), $W \to \ell\nu$ (1L), $Z \to \ell\ell$ (2L) [$\ell$ = e, μ]
- Main backgrounds
  - V + jets, single and pair production of top quarks, dibosons
  - VH($H \to bb$): small but largely irreducible
- Baseline event selections
  - (high-$p_T$) vector boson recoiling against a Higgs boson candidate
  - veto events with high jet multiplicity to suppress tt contribution (0L & 1L)
- Previous result (36 $fb^{-1}$): [JHEP 03 (2020) 131]
- **Today: result with the full Run 2 data set (138 $fb^{-1}$)** *arXiv:2205.05550 (submitted to PRL)*

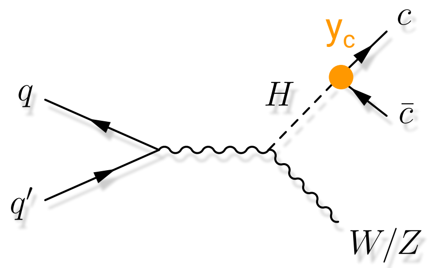


*JHEP 03 (2020) 131*

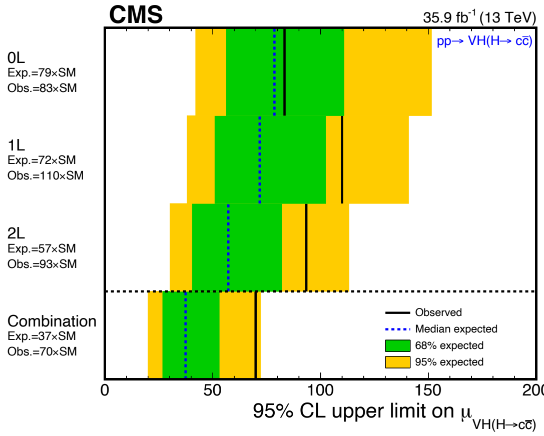


*Corresponding ATLAS analysis: arXiv:2201.11428. See also recent LHC seminar by A. Chisholm.*

# Analysis overview

- Two complementary approaches for Higgs boson candidate reconstruction

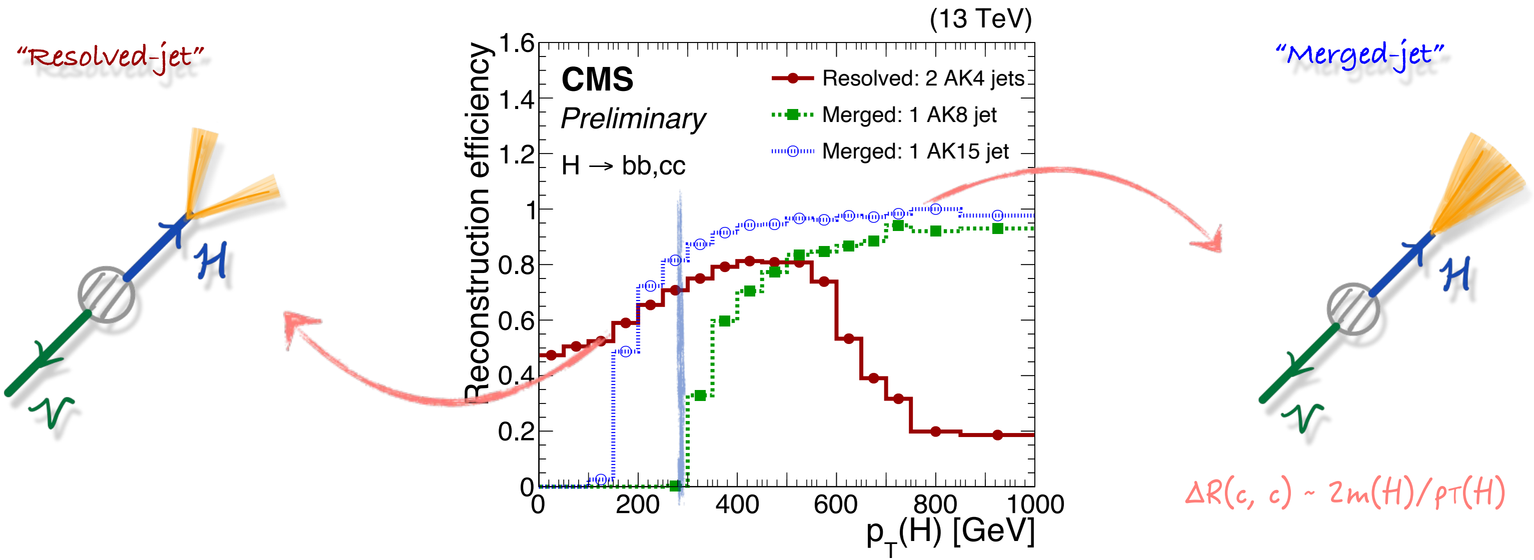


- **Resolved-jet topology**
  - reconstructs H → cc decay with two small-R jets (R=0.4, "AK4")
  - probes the bulk (>95%) of the signal phase space
- **Merged-jet topology**
  - reconstructs H → cc decay with one large-R jets (R=1.5, "AK15")
  - small signal acceptance (<5%) but higher purity
  - better exploits the correlation between the two charm quarks

# Merged-jet topology

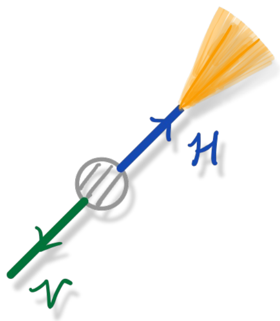

# H → cc identification

- ❑ Merged-jet topology: Higgs boson candidate reconstructed via a single large-R jet ($p_T$ > 300 GeV)
- ❑ A major improvement: **ParticleNet** tagger used to identify H → cc decay

JHEP 03 (2020) 131 (2016 analysis)

**DeepAK8 (DeepAK15)** [JINST 15 (2020) P06005]
- multi-class DNN boosted jet classifier
- directly uses jet constituents (particle-flow candidates / secondary vertices)
- 1D convolutional neural network
- mass decorrelation via adversarial training

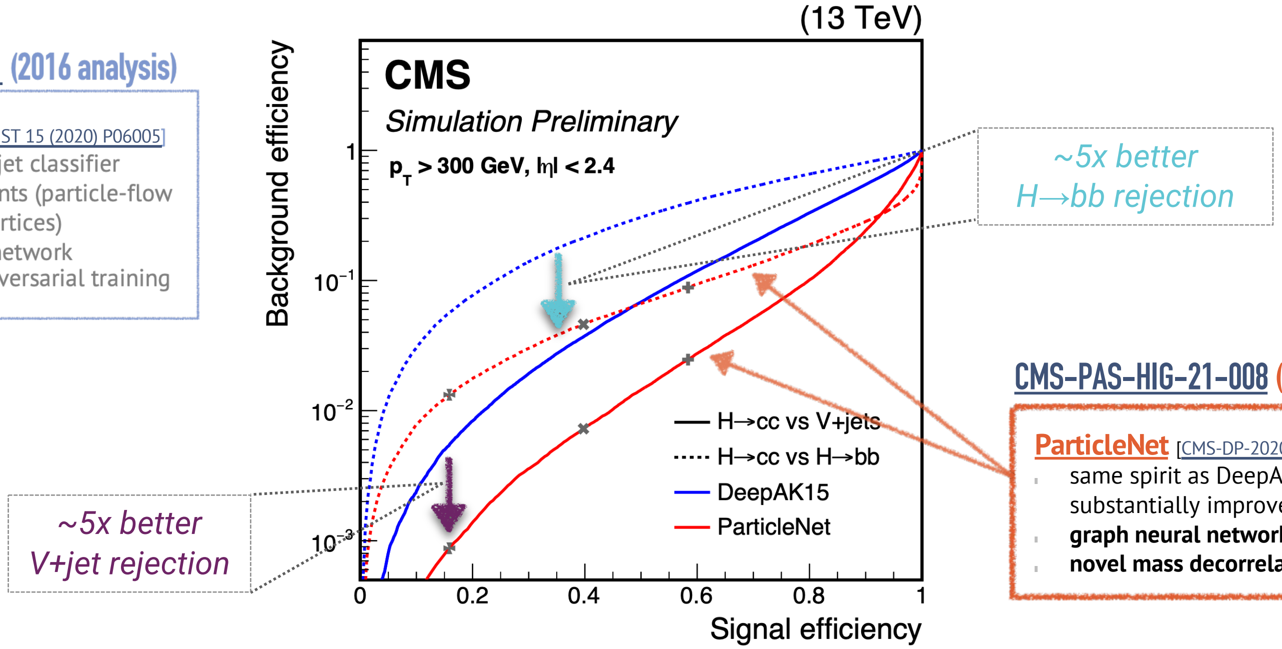


CMS-PAS-HIG-21-008 (Run 2 analysis)

**ParticleNet** [CMS-DP-2020-002]
- same spirit as DeepAK8, but substantially improved:
- **graph neural network architecture**
- **novel mass decorrelation technique**

*>2x improvement in the final sensitivity*

# ParticleNet architecture

- New jet representation: "particle cloud"
  - treating a jet as an unordered set of particles, distributed in the $\eta - \varphi$ space

- ParticleNet [H. Qu and L. Gouskos, Phys.Rev.D 101 (2020) 5, 056019]
  - graph neural network architecture adapted from DGCNN [arXiv:1801.07829]
  - permutation-invariant architecture leads to significant performance improvement

*Image from arXiv:2202.03772*

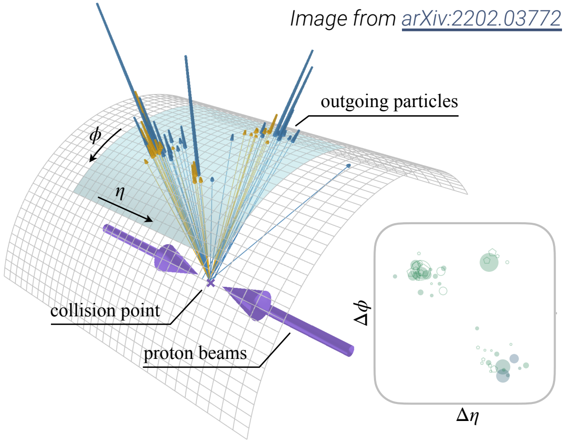


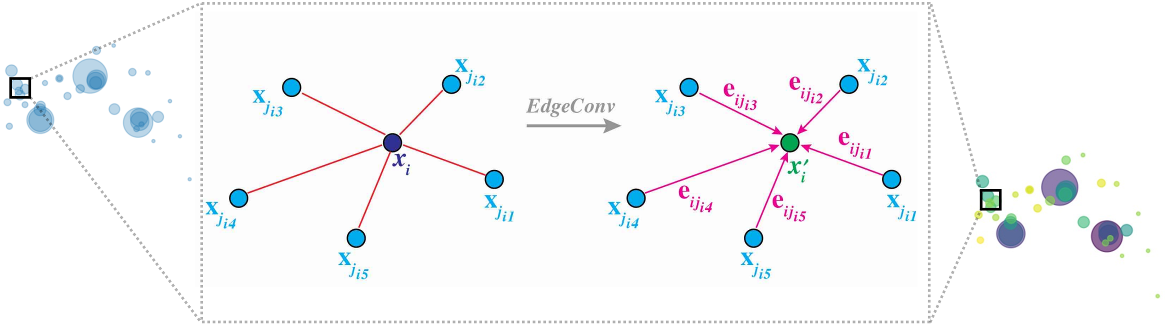


*Performance on top quark tagging benchmark [SciPost Phys. 7, 014 (2019)]*

| | $1/\varepsilon_b$ at $\varepsilon_s = 30\%$ |
|---|---|
| ResNeXt-50 | $1147 \pm 58$ |
| P-CNN | $759 \pm 24$ |
| PFN | $888 \pm 17$ |
| ParticleNet-Lite | $1262 \pm 49$ |
| ParticleNet | $\mathbf{1615 \pm 93}$ |

# Mass decorrelation

CMS-DP-2020-002

*Plain training: no mass decorrelation*

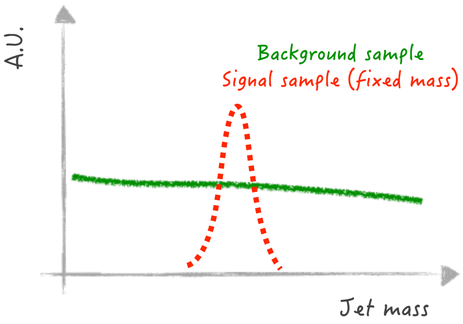


*Mass-decorrelated training*

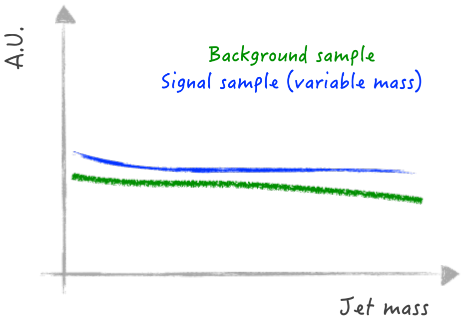


*Background jet mass*

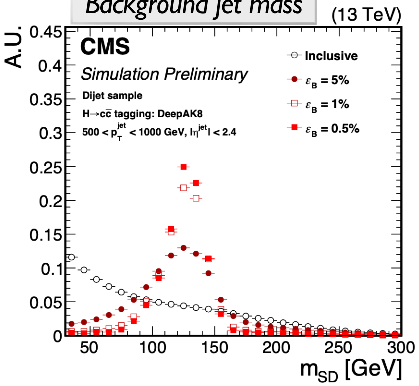


*Background jet mass*

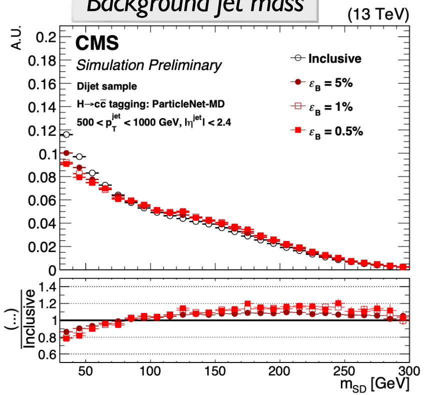


- ❑ "Mass sculpting": background jet mass shape becomes similar to signal after tagger selection
- ❑ New approach to prevent mass sculpting
  - using a special signal sample for training
    - hadronic decays of a spin-0 particle X
      - $X \rightarrow bb$, $X \rightarrow cc$, $X \rightarrow qq$
    - not a fixed mass, but a **flat mass spectrum**
      - $m(X) \in [15, 250]$ GeV
  - allows to easily reweight both signal and background to a ~flat 2D distribution in ($p_T$, mass) for the training
- ❑ Signal and background have the same (~flat) mass spectrum, thus no sculpting will develop in the training

# Mass decorrelation (II)

CMS-DP-2020-002

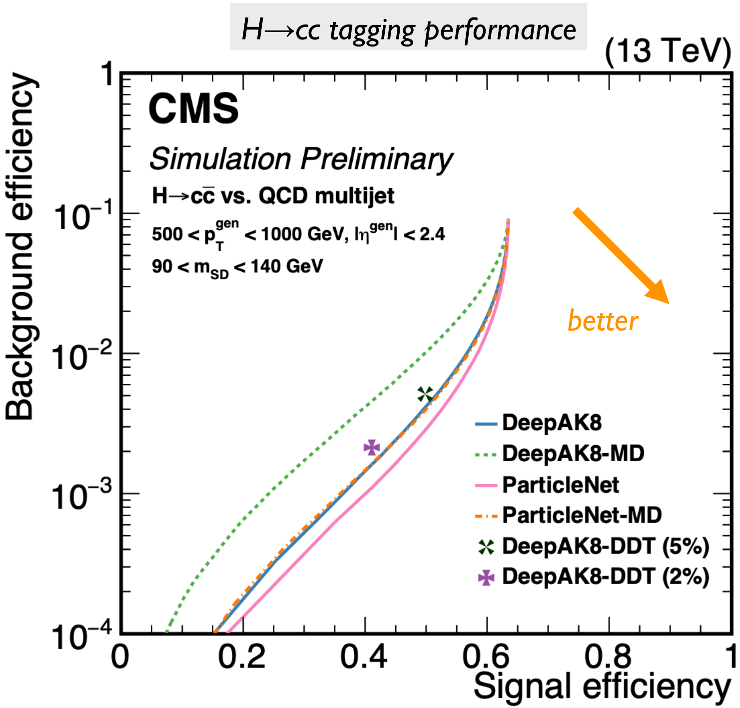


- "Mass sculpting": background jet mass shape becomes similar to signal after tagger selection
- New approach to prevent mass sculpting
  - using a special signal sample for training
    - hadronic decays of a spin-0 particle X
      - X → bb, X → cc, X → qq
    - not a fixed mass, but a **flat mass spectrum**
      - m(X) ∈ [15, 250] GeV
  - allows to easily reweight both signal and background to a ~flat 2D distribution in ($p_T$, mass) for the training
- Performance loss due to mass decorrelation greatly reduced compared to the previous approach (DeepAK8-MD, based on "adversarial training")

# Calibration of the cc-tagger

- ❑ Need to measure ParticleNet cc-tagging efficiency in data
  - no pure sample of H → cc jets (or even Z → cc) in data
  - using g → cc in QCD multi-jet events as a proxy
- ❑ Difficulty: select a phase-space in g → cc that resembles H → cc
  - solution: a **dedicated BDT** developed to distinguish **hard 2-prong splittings** (*i.e., high quark contribution to the jet momentum*) from **soft cc radiations** (*i.e., high gluon contribution to the jet momentum*)
  - also allows to adjust the similarity between proxy and signal jets
    - by varying the sfBDT cut — treated as a systematic uncertainty
- ❑ Perform a fit to the secondary vertex mass shapes in the "passing" and "failing" regions simultaneously to extract the scale factors
  - three templates: cc (+ single c), bb (+ single b), light flavor jets
- ❑ Derived cc-tagging scale factors typically 0.9—1.3
  - corresponding uncertainties are 20—30%

CMS-DP-2022-005

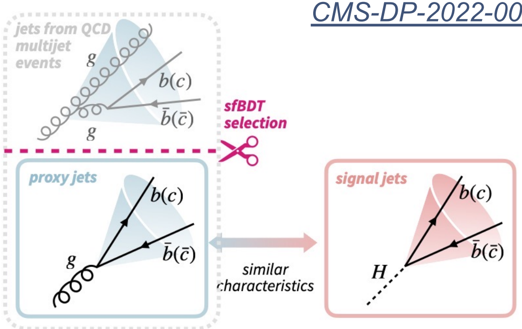


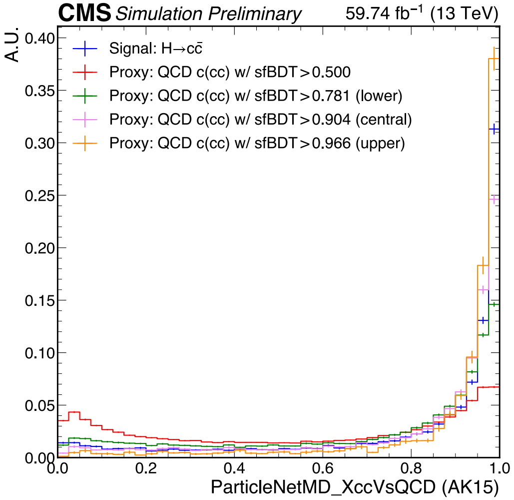

# Large-R jet mass regression

CMS DP-2021/017

- Jet mass: one of the most powerful observable to distinguish signal and backgrounds
- New ParticleNet-based regression algorithm to improve the large-R jet mass reconstruction
  - training setup similar to the ParticleNet tagger; the regression target:
    - signal (X → bb/cc/qq): generated particle mass of X [flat spectrum in 15 – 250 GeV]
    - background (QCD) jets: soft drop mass of the particle-level jet

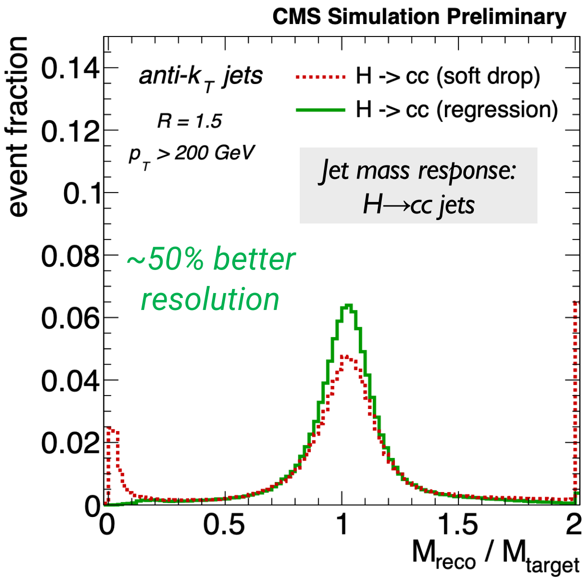


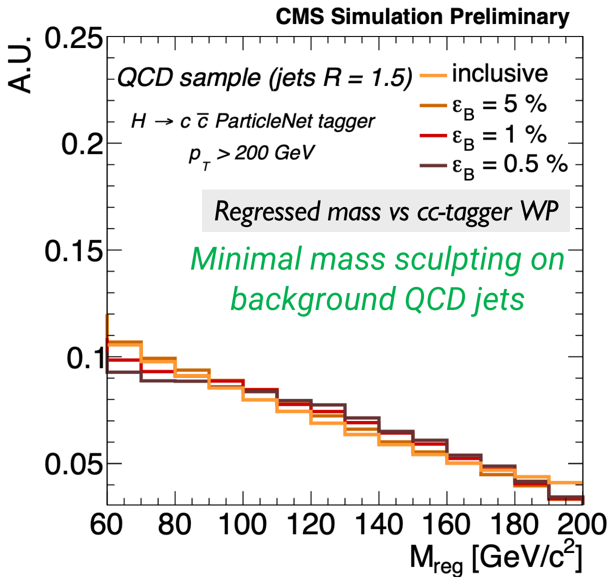


*20 – 25% improvement in the final sensitivity*

# Analysis strategy

- Factorized approach for analysis design
  - event-level **kinematic BDT** developed in each channel to better suppress main backgrounds (V+jets, tt)
    - using only *event kinematics*, no intrinsic properties (e.g., mass/flavor) of the large-R jet
  - **ParticleNet cc-tagger** then used to define 3 cc-flavor enriched regions and reject light/bb-flavor jets
  - finally: fit to the **ParticleNet-regressed large-R jet mass** shape for signal extraction
- Kinematic BDT, ParticleNet cc-tagger and regressed jet mass largely independent of each other
  - allowing for a simple and robust strategy for background estimation and signal extraction

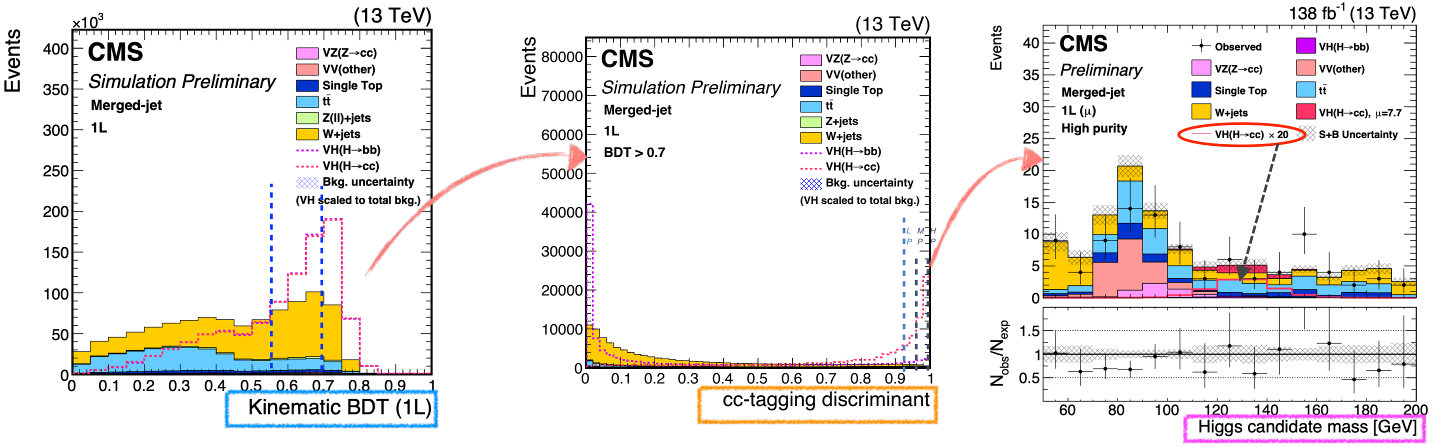

# Background estimation

- Normalizations of main backgrounds estimated via dedicated data control regions (CRs)
  - V+jets CR: use the low kinematic BDT region
  - tt CR (0L & 1L): invert the cut on the number of additional small-R jets (i.e., $N_{aj} \geq 2$)
  - free-floating parameters scale the normalizations in CRs and signal regions (SRs) simultaneously

- CRs designed to have similar jet flavor composition as the SR
  - flavor-independent kinematic BDT + same cc-tagging requirement in CRs as in SR
  - allows to correct cc-tagging efficiency for backgrounds directly from data
  - cc-tagging SFs only needed for the signal VH(H → cc) process (and VZ(Z → cc))
    - conservative uncertainty (2x/0.5x) for the misidentification of H(Z) → bb as H(Z) → cc

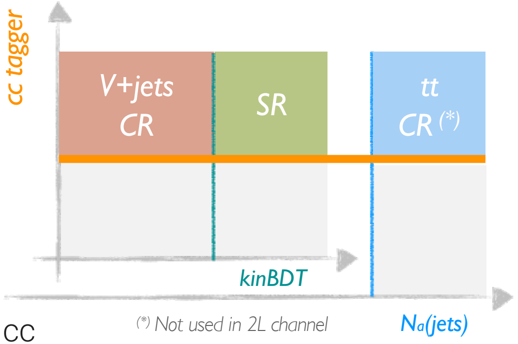


- Minor backgrounds (single top, dibosons, VH(H → bb)) estimated from simulation
  - dibosons: applying differential NNLO QCD + NLO EW corrections as a function of $p_T(V)$ [JHEP 2002 (2020) 087]

# Resolved-jet topology

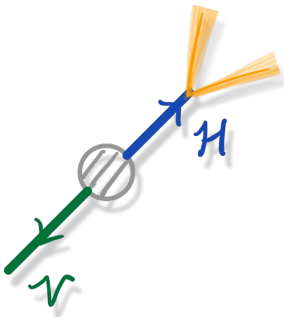

# Charm quark identification

- Resolved-jet topology: Higgs boson candidate reconstructed with two small-R jets

JINST 17 (2022) P03014

- Charm quark jet identification: **DeepJet** algorithm
  - ~2x (~40%) improvement in light (b) jet rejection at 40% c jet efficiency compared to DeepCSV

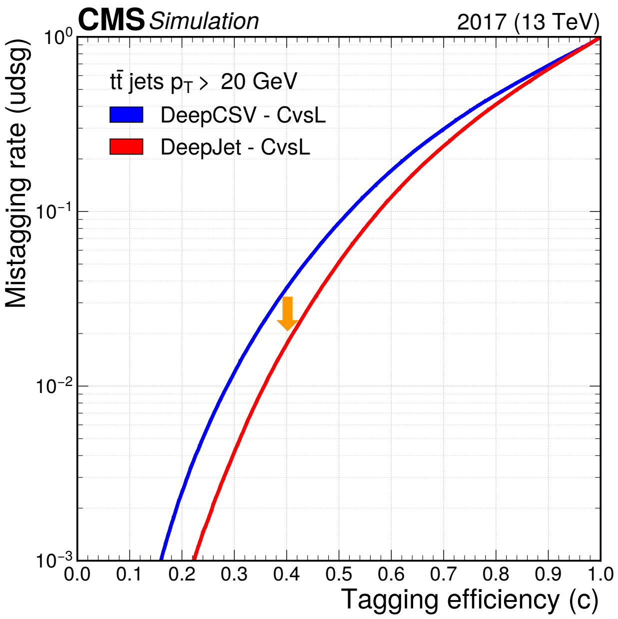


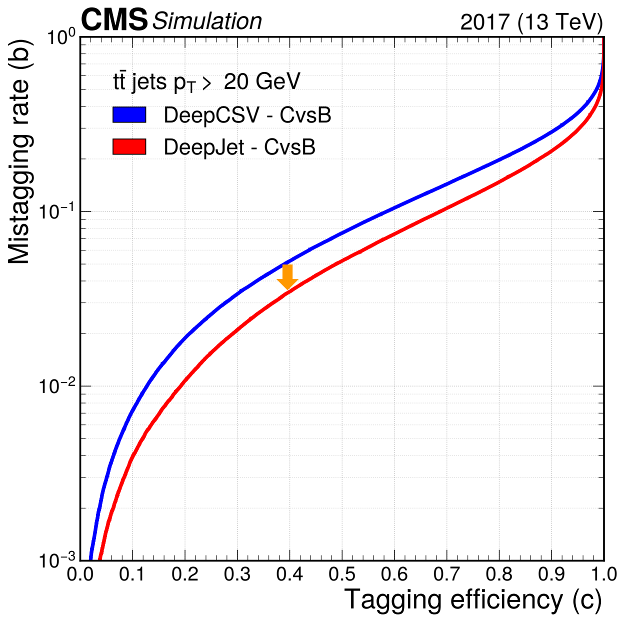

# Charm tagging calibration

*JINST 17 (2022) P03014*

- Novel calibration method to correct the entire distributions of the c-tagging discriminants
  - per-jet SFs derived as a function of (CvsL, CvsB | truth flavor)
- SFs derived with an iterative approach using three samples
  - Z(ℓℓ) + jets (light jet enriched); W + c (c-jet enriched); tt (b-jet enriched)

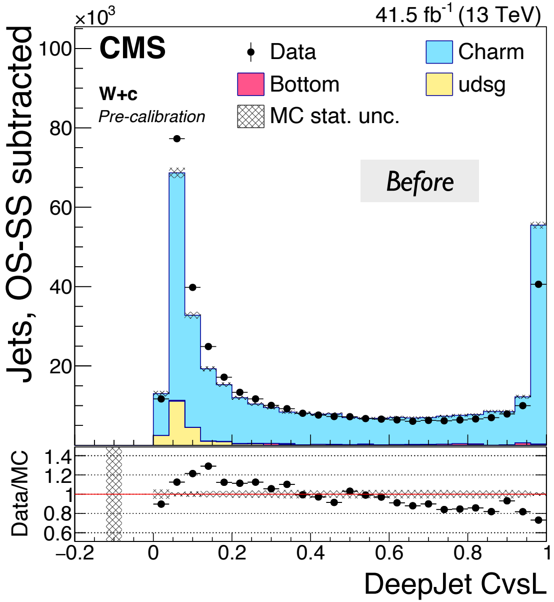


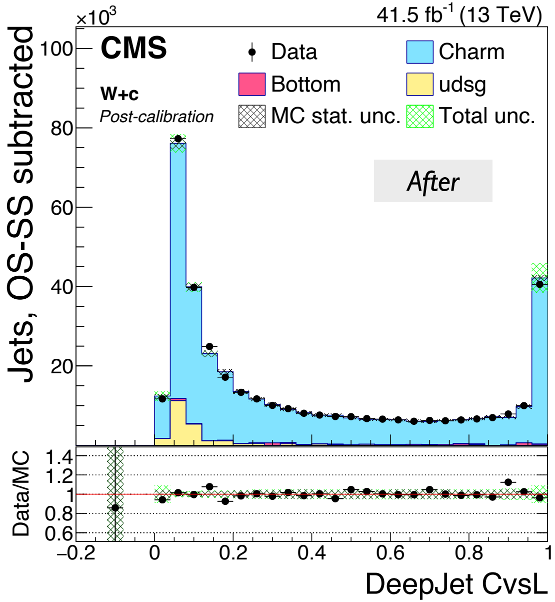


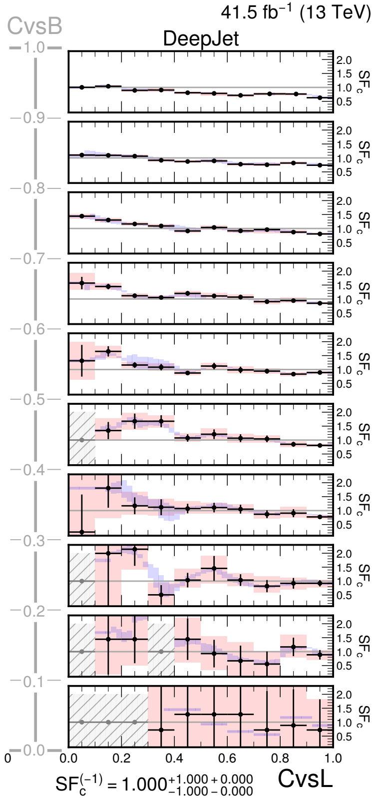

# Charm jet energy regression

- Dedicated jet energy regression algorithm developed to improve the c-jet energy scale and resolution
  - based on the b jet energy regression [Comput.Softw.Big Sci. 4 (2020) 10] used in several CMS H→bb analyses
  - re-trained for c jets instead of b jets
    - c jets collected from W→cx decay in tt MC events
  - provides simultaneous estimation of the c jet energy and its resolution
    - both used as inputs to the signal extraction BDT

***Inputs***

**43 high-level features:**

- jet kinematics
- jet composition
- pileup information
- semi-leptonic decays
- secondary vertex

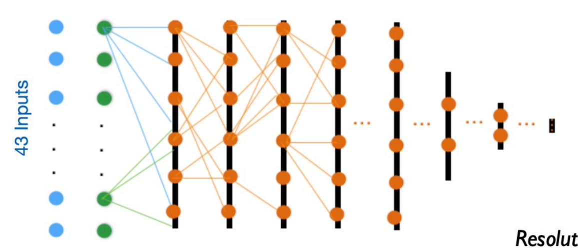


***Outputs***

- $\hat{y} = p_T(\text{gen})/p_T(\text{reco})$
- $\hat{y}_{0.25}$: 25% quantile
- $\hat{y}_{0.75}$: 75% quantile

*Resolution estimator:* $\hat{\sigma} \equiv \frac{1}{2}(\hat{y}_{75\%} - \hat{y}_{25\%})$

**Joint loss function for correction (Huber) and resolution (quantiles) :**

$$Loss = Huber(y, F(x)) + \rho_{0.75}(y - F(x)) + \rho_{0.25}(y - F(x))$$

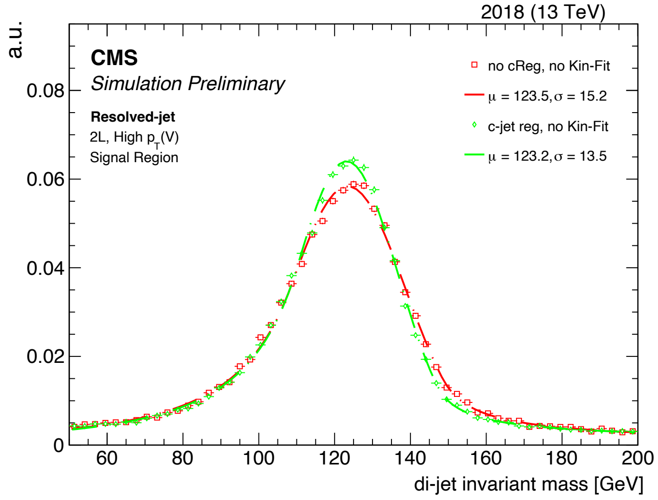

# Higgs boson candidate reconstruction

- Higgs boson candidate reconstructed using the two small-R jets with highest CvsL scores
- To improve the Higgs candidate mass resolution:
  - recovery of final state radiations (FSR)
    - additional jets within $\Delta R < 0.8$ from either of the two selected jets are included in the calculation of the Higgs candidate's 4-momentum
    - improves the Higgs mass resolution by a few percent
  - new DNN-based c-jet energy regression
    - ~20% improvement in Higgs candidate mass resolution
  - improved kinematic fit in the 2L channel
    - better reconstruction of the Higgs candidate's 4-momentum using constraints from the $Z \to \ell\ell$ system
    - up to 30% improvement in Higgs candidate mass resolution

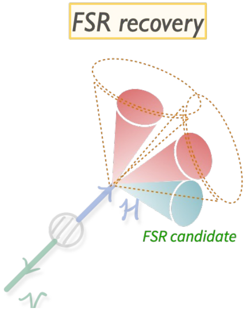


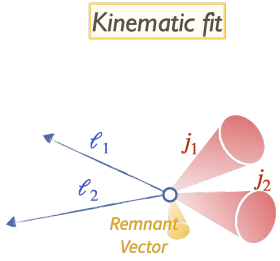


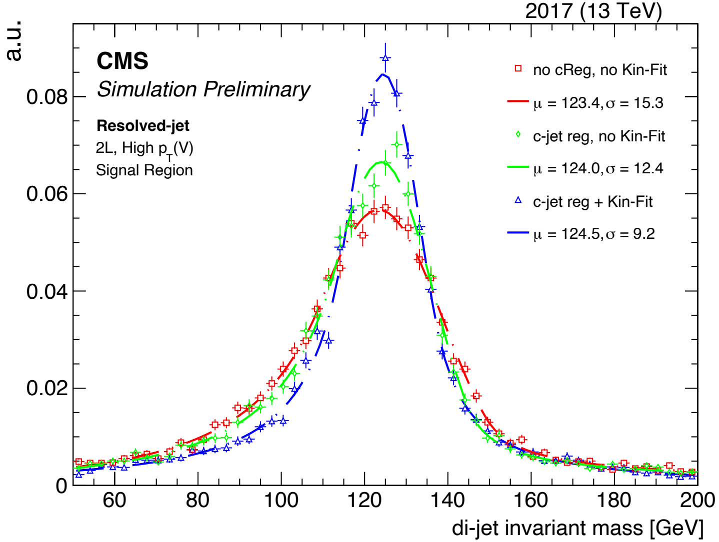

# Signal extraction strategy

- Event-level BDT trained in each channel to maximize the signal vs background separation
  - inputs: event kinematics, Higgs candidate properties, c-tagging discriminants
    - + kinematic fit variables in 2L
- Background estimation
  - dedicated CRs to constrain the normalizations of main backgrounds (V + jets, tt)
    - V + jets split based on flavor: V + b, V + c, V + udsg
- Simultaneous fit of SRs (BDT shapes) and CRs (c-tagging discriminants) for signal extraction

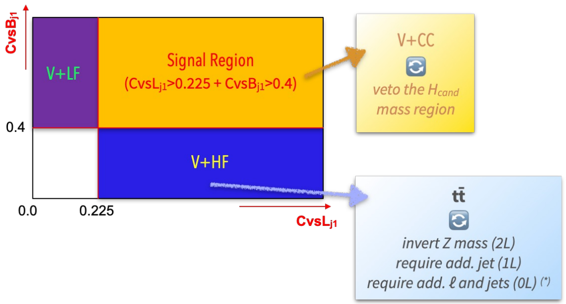


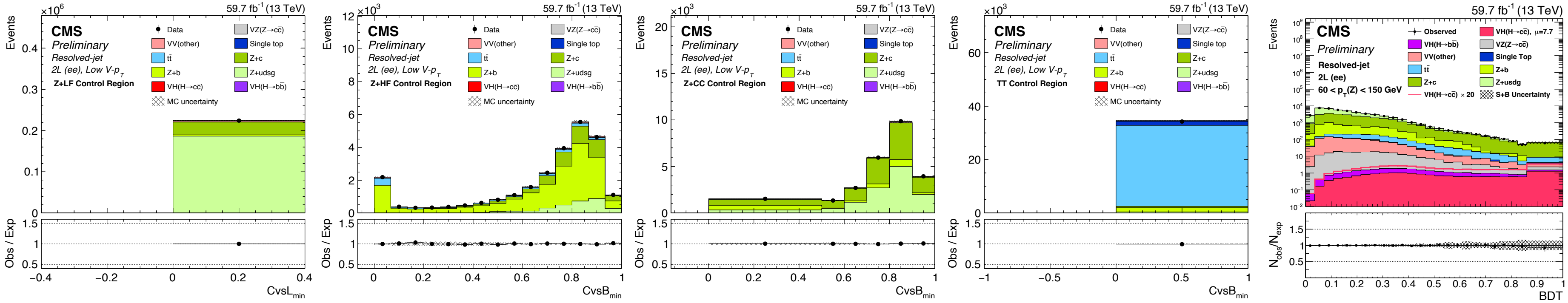

# Results

# Combination of the two topologies

- The two topologies are made orthogonal via the presence of large-R jet with $p_T$ > 300 GeV
  - $p_T$ threshold chosen to maximize expected sensitivity

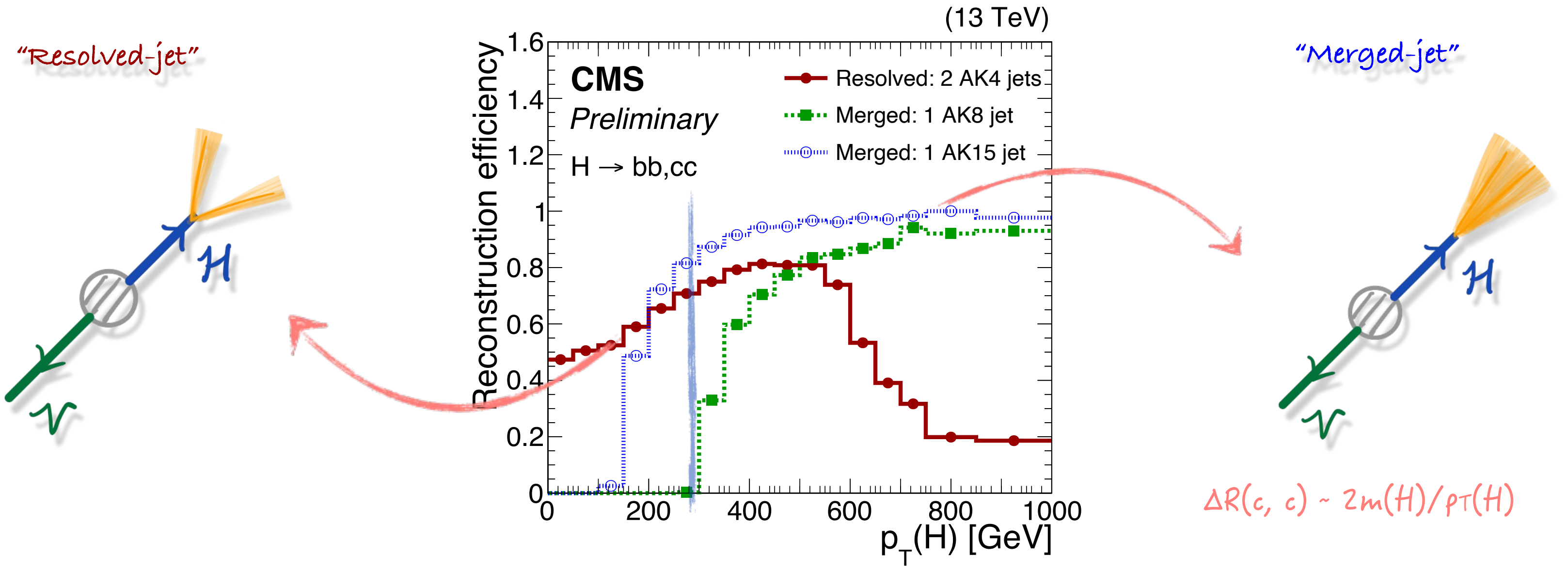

# Uncertainties

- Systematic uncertainties correlated between topologies, except:
  - background normalizations for V+jets and tt
  - charm quark identification efficiencies

*Relative contributions to the total uncertainty on $\mu$*

| Uncertainty source | $\Delta\mu / (\Delta\mu)_{tot}$ |
|---|---|
| **Statistical** | **85%** |
| Background normalizations | 37% |
| **Experimental** | **48%** |
| Sizes of the simulated samples | 37% |
| Charm identification efficiencies | 23% |
| Jet energy scale and resolution | 15% |
| Simulation modeling | 11% |
| Luminosity | 6% |
| Lepton identification efficiencies | 4% |
| **Theory** | **22%** |
| Backgrounds | 17% |
| Signal | 15% |

- Main uncertainties
  - limited statistics of the data set
  - size of simulated samples (especially NLO V+jets)
  - charm quark identification efficiencies

# VZ(Z → cc) results

- The full analysis procedure is validated by measuring the VZ(Z → cc) process
  - resolved-jet topology:
    - BDT re-trained using VZ(Z → cc) as signal
    - fit to the BDT shapes to extract the signal
  - merged-jet topology:
    - no change to the analysis procedure
    - fit to the large-R jet mass shapes to extract the signal

# VZ(Z → cc) results

❑ The full analysis procedure is validated by measuring the VZ(Z → cc) process

arXiv:2205.05550

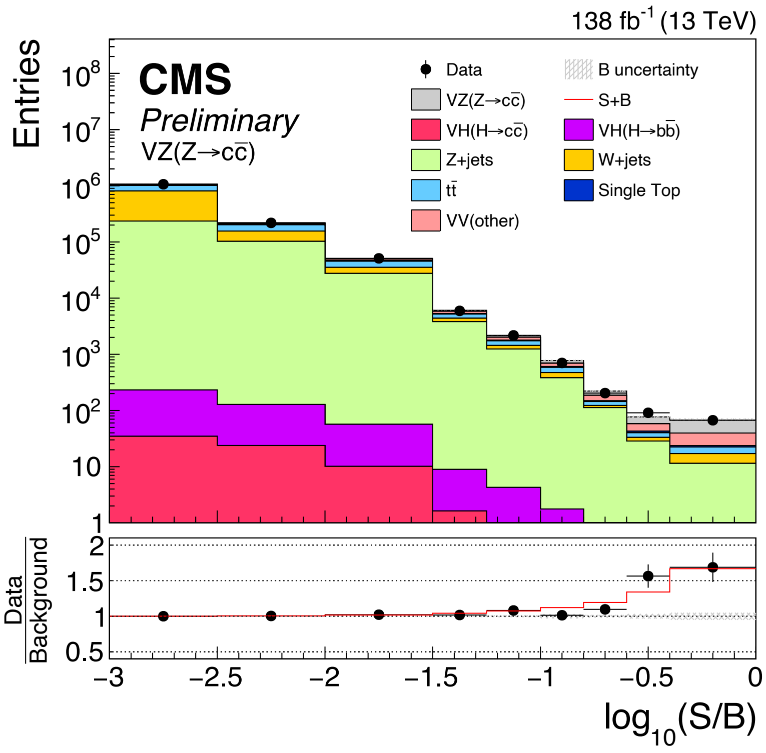


Observed significance for VZ(Z → cc): **5.7σ**

- expected significance: 5.9σ

**First observation of Z→cc at a hadron collider!**

# VZ(Z → cc) results

- The full analysis procedure is validated by measuring the VZ(Z → cc) process

arXiv:2205.05550

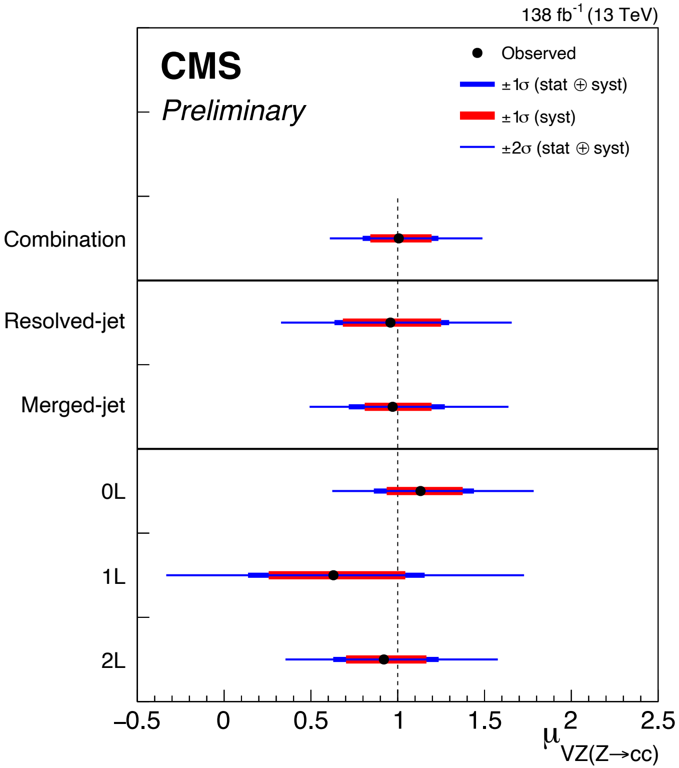


Best-fit signal strength: $\mu_{VZ(Z\to cc)} = 1.01^{+0.23}_{-0.21}$

- very good agreement with SM expectation
- consistent results between topologies/channels

# VH(H → cc) results

❑ Post-fit distributions in the two topologies and the combination

arXiv:2205.05550

*Merged-jet topology*

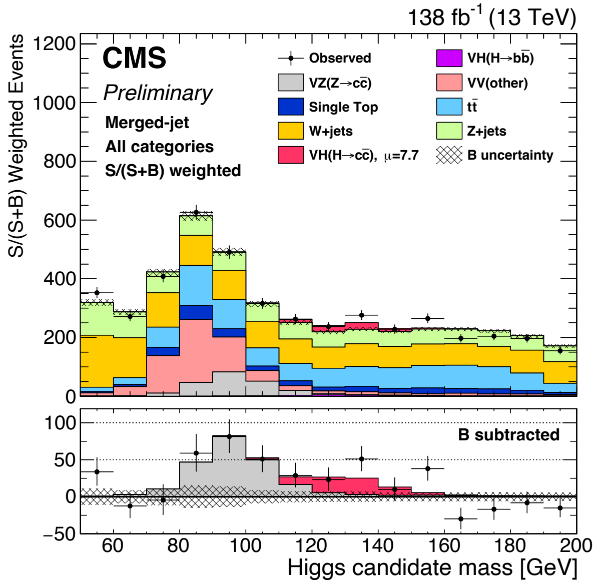


*Resolved-jet topology*

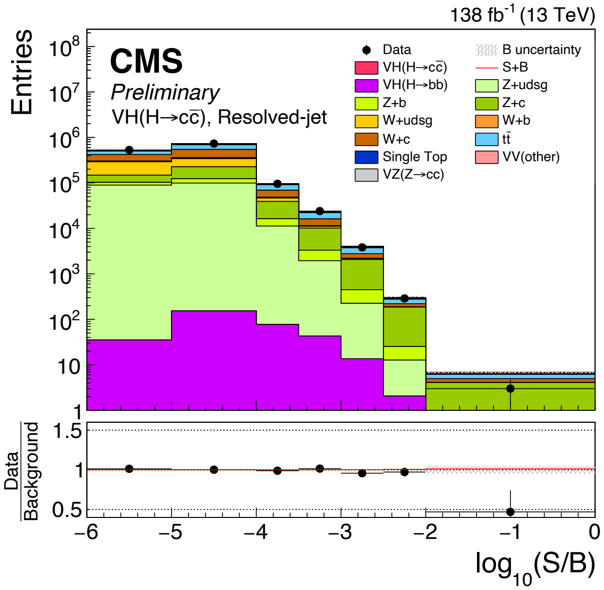


*Combination*

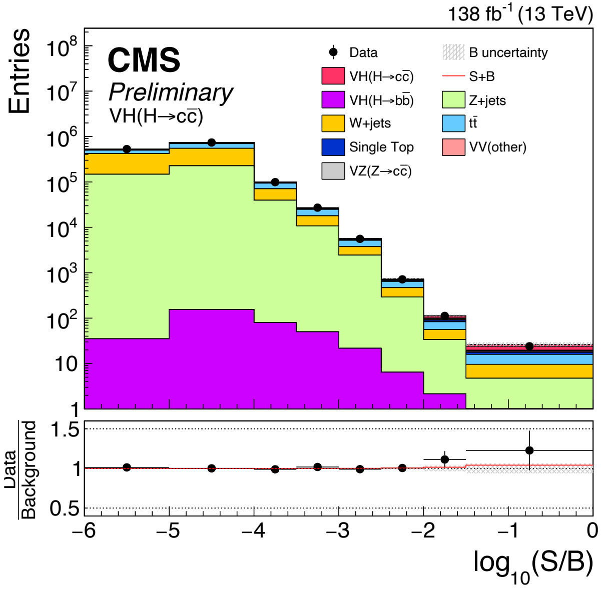

# VH(H → cc) results



- Upper limits on the VH(H → cc) signal strength at 95% CL:
  - **$\mu_{VH(H\to cc)}$ < 14 (7.6) observed (expected)**
  - substantially stronger than ATLAS full Run 2 result
    - $\mu_{VH(H\to cc)}$ < 26 (31) obs. (exp.) [arXiv:2201.11428]
- Best fit signal strength
  - $\mu_{VH(H\to cc)} = 7.7^{+3.8}_{-3.5}$
  - consistent with the SM prediction within 2σ

arXiv:2205.05550

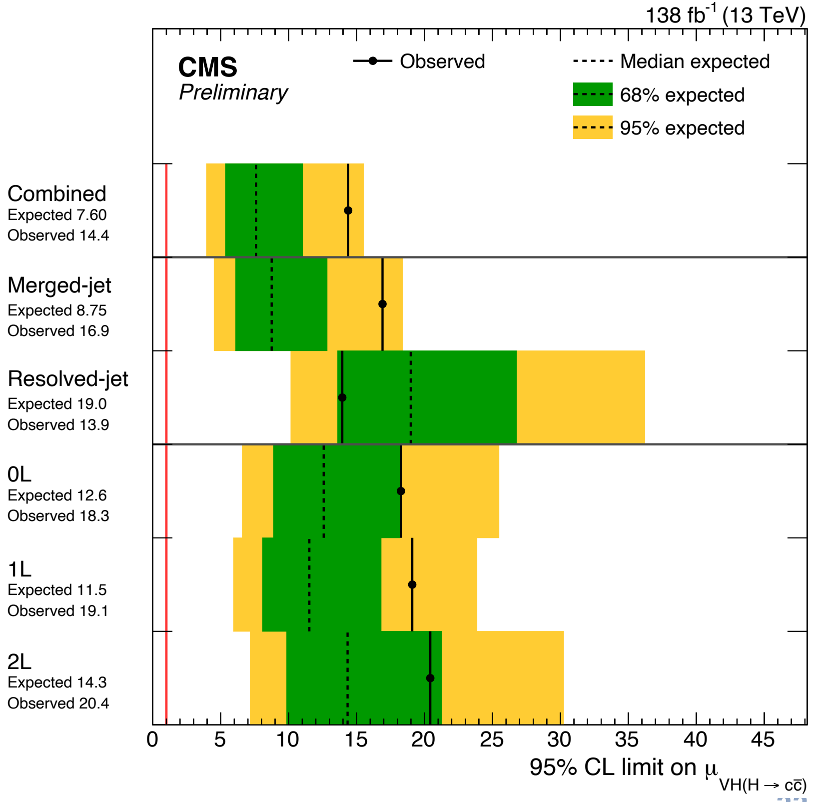

# VH(H → cc) results



- Results used to set a constraint on the charm quark Yukawa coupling modifier $\kappa_c = y_c / y_c^{SM}$
  - for simplicity, only considering effects on B(H→cc) and fixing all other couplings at SM values:

$$\mu_{VH(H\to c\bar{c})} = \frac{\kappa_c^2}{1 + \mathcal{B}_{SM}(H \to c\bar{c}) \times (\kappa_c^2 - 1)}.$$

- The 95% CL interval on $\kappa_c$:
  - observed: **$1.1 < |\kappa_c| < 5.5$**
  - expected: **$|\kappa_c| < 3.4$**
  - **most stringent constraint on $\kappa_c$ to date!**
    - comparable to the previous projection for HL-LHC w/ 3000 $fb^{-1}$: $|\kappa_c| < 3.0$ [ATL-PHYS-PUB-2021-039]

arXiv:2205.05550

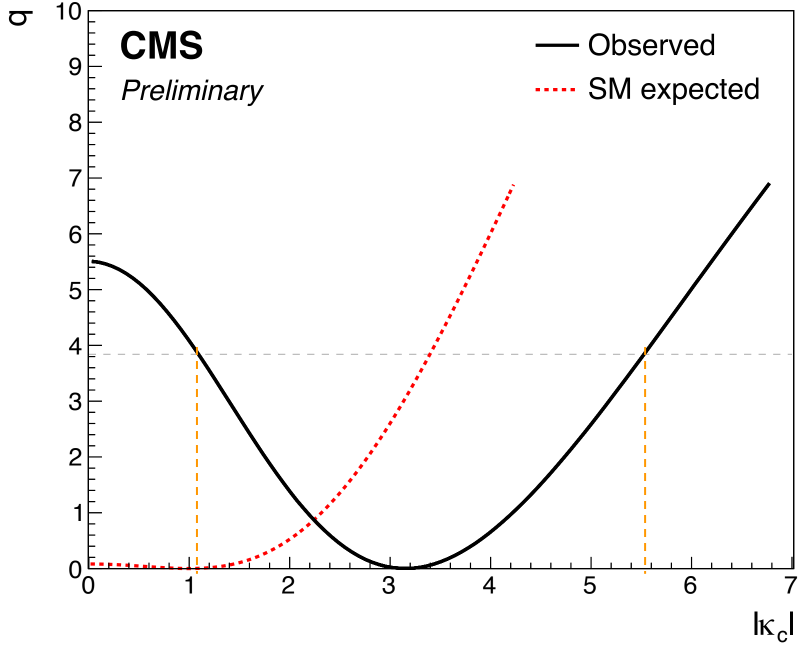

# Prospects: HL-LHC

# Projection at HL-LHC: Setup

- Extrapolation of the merged-jet analysis to HL-LHC with 3000 $fb^{-1}$ data
- Modifications to the Run 2 analysis to allow for a simultaneous constraint on $H \to bb$ and $H \to cc$
  - addition of 3 categories enriched in $H \to bb$ decays, selected with the ParticleNet bb-tagging discriminant
    - very small (1-2%) overlap of bb and cc categories – events assigned to a unique category
  - large-R jet $p_T$ threshold lowered from 300 GeV to 200 GeV – increasing signal acceptance

- Systematic uncertainties adjusted according to the Yellow Report [CERN-2019-007]
  - theoretical uncertainties: reduced by half
  - most experimental uncertainties: scaled down with $\sqrt{\mathcal{L}}$
    - bb and cc tagging efficiencies: constrained by $VZ(Z \to bb)$ and $VZ(Z \to cc)$ events to ~3% and ~5%
    - misidentification of $H \to bb$ as $H \to cc$: a prominent uncertainty on $H \to cc$ measurement at HL-LHC
      - assumed to be reduced from ~100% (Run 2) to 20% in the projection

# Projection at HL-LHC

- Simultaneous extraction of the $H \rightarrow bb$ and $H \rightarrow cc$ signal strengths

CMS-PAS-HIG-21-008

  - $\mu_{VH(H\rightarrow bb)} = 1.00 \pm 0.03\ (stat.) \pm 0.04\ (syst.) = 1.00 \pm 0.05\ (total)$
  - $\mu_{VH(H\rightarrow cc)} = 1.0 \pm 0.6\ (stat.) \pm 0.5\ (syst.) = 1.0 \pm 0.8\ (total)$

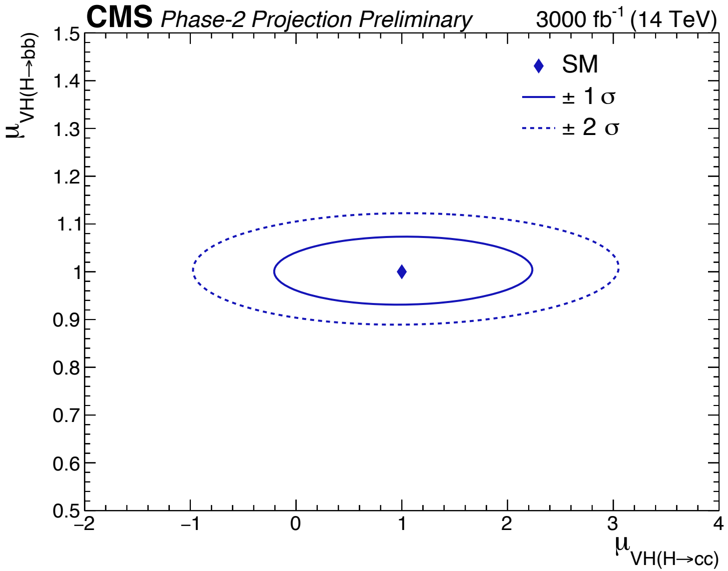


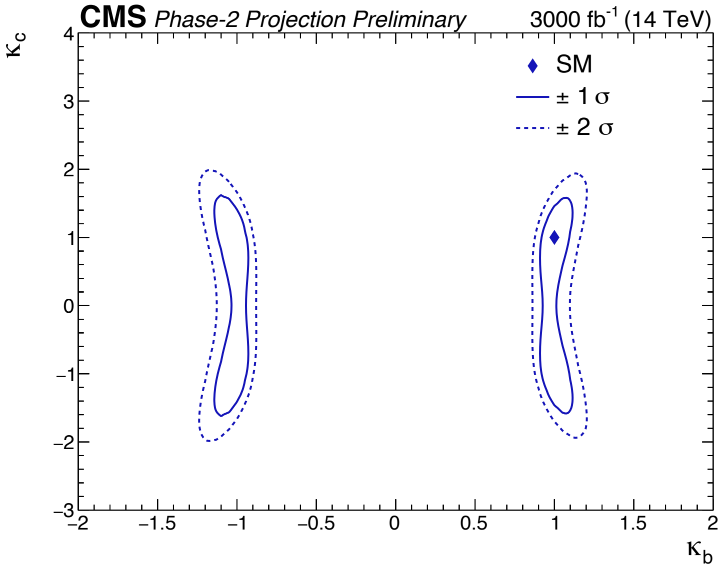


***Expected sensitivity approaches the SM value for the Higgs-charm coupling.***

# Prospects: ML for jet tagging

# Beyond ParticleNet

- **Particle Transformer (ParT)**: a new Transformer-based architecture for jet tagging
  - Transformer + *interaction*

*H. Qu, C. Li, S. Qian,*
*arXiv:2202.03772*
*GitHub*

*Interaction features*

$$\Delta = \sqrt{(y_a - y_b)^2 + (\phi_a - \phi_b)^2},$$
$$k_{\mathrm{T}} = \min(p_{\mathrm{T},a}, p_{\mathrm{T},b})\Delta,$$
$$z = \min(p_{\mathrm{T},a}, p_{\mathrm{T},b})/(p_{\mathrm{T},a} + p_{\mathrm{T},b}),$$
$$m^2 = (E_a + E_b)^2 - \|\mathbf{p}_a + \mathbf{p}_b\|^2,$$

*Motivated by LundNet [F. Dreyer and H. Qu, JHEP 03 (2021) 052]*

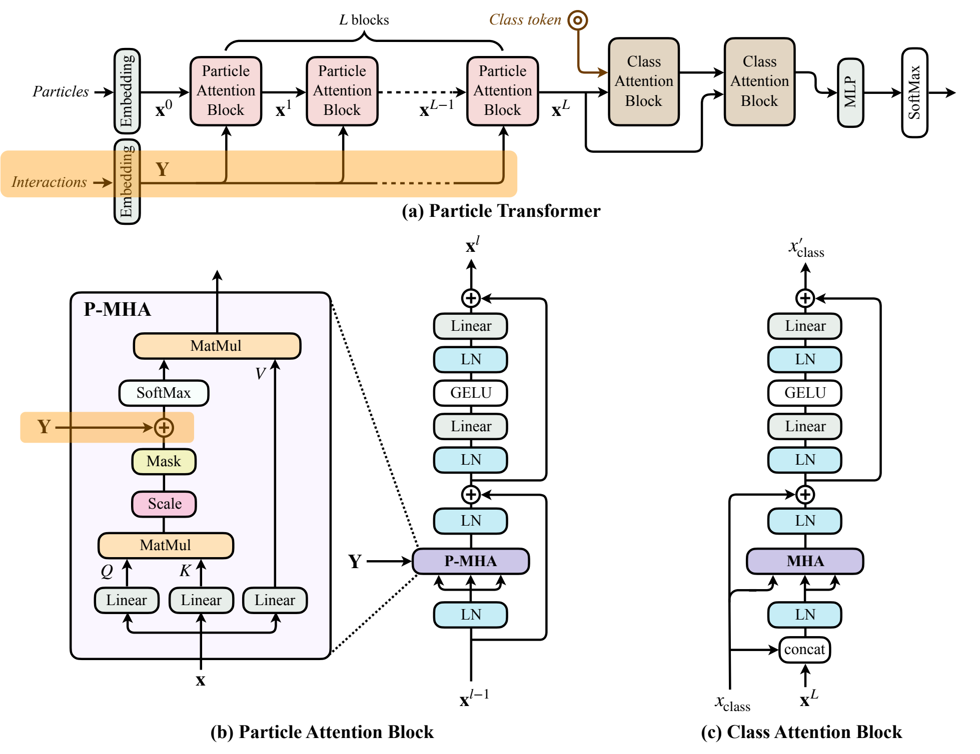

# Beyond ParticleNet: JetClass dataset

- A new large-scale public jet dataset: 100M jets in 10 classes
  - MadGraph + Pythia (Herwig) + Delphes

H. Qu, C. Li, S. Qian,
arXiv:2202.03772
GitHub

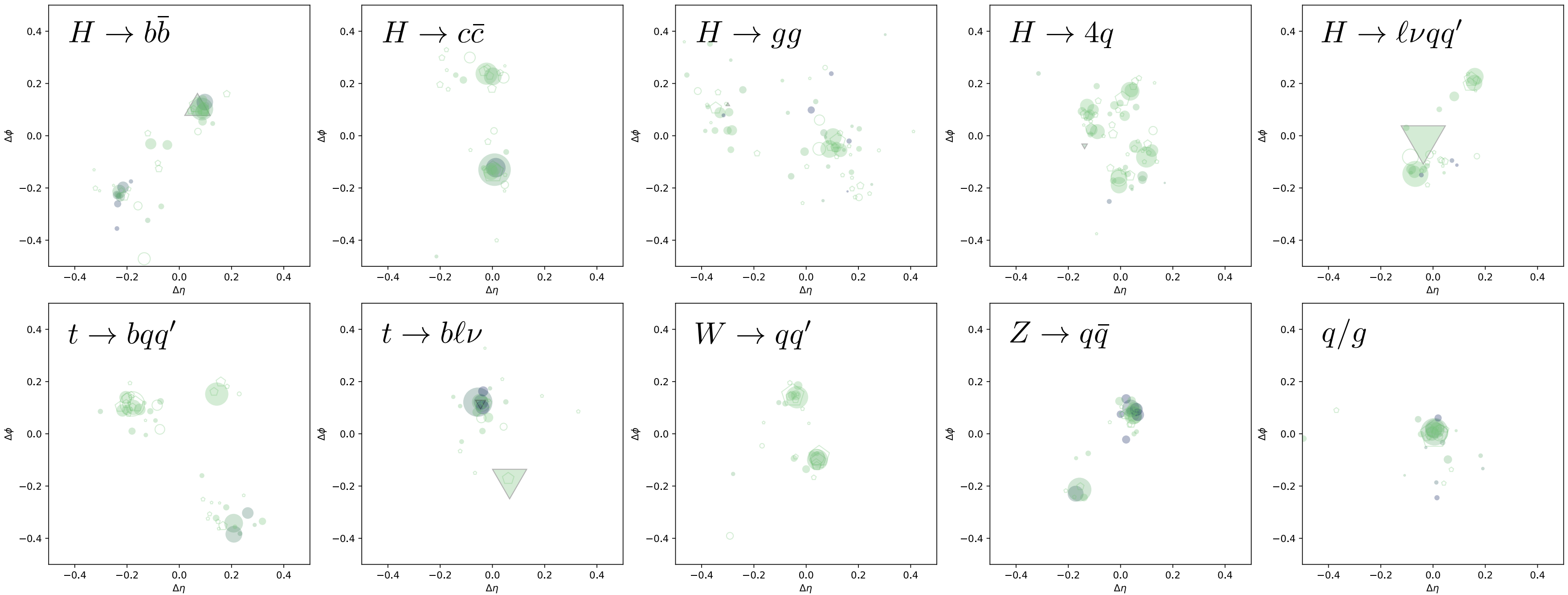

# Beyond ParticleNet: Particle Transformer

H. Qu, C. Li, S. Qian, arXiv:2202.03772, GitHub

$Rej_{50\%} = 1/\varepsilon_{bkg}$ @ $\varepsilon_{sig} = 50\%$

*Performance comparison on the JetClass dataset*

| | All classes | | $H \to b\bar{b}$ | $H \to c\bar{c}$ | $H \to gg$ | $H \to 4q$ | $H \to \ell\nu qq'$ | $t \to bqq'$ | $t \to b\ell\nu$ | $W \to qq'$ | $Z \to q\bar{q}$ |
|---|---|---|---|---|---|---|---|---|---|---|---|
| | Accuracy | AUC | $Rej_{50\%}$ | $Rej_{50\%}$ | $Rej_{50\%}$ | $Rej_{50\%}$ | $Rej_{99\%}$ | $Rej_{50\%}$ | $Rej_{99.5\%}$ | $Rej_{50\%}$ | $Rej_{50\%}$ |
| PFN | 0.772 | 0.9714 | 2924 | 841 | 75 | 198 | 265 | 797 | 721 | 189 | 159 |
| P-CNN | 0.809 | 0.9789 | 4890 | 1276 | 88 | 474 | 947 | 2907 | 2304 | 241 | 204 |
| ParticleNet | 0.844 | 0.9849 | 7634 | 2475 | 104 | 954 | 3339 | 10526 | 11173 | 347 | 283 |
| **ParT** | **0.861** | **0.9877** | **10638** | **4149** | **123** | **1864** | **5479** | **32787** | **15873** | **543** | **402** |
| ParT (plain) | 0.849 | 0.9859 | 9569 | 2911 | 112 | 1185 | 3868 | 17699 | 12987 | 384 | 311 |

*Fine-tuning result on Top-tagging Benchmark (~2M jets)* [SciPost Phys. 7 (2019) 014]

| | Accuracy | AUC | $Rej_{50\%}$ | $Rej_{30\%}$ |
|---|---|---|---|---|
| P-CNN | 0.930 | 0.9803 | $201 \pm 4$ | $759 \pm 24$ |
| PFN | — | 0.9819 | $247 \pm 3$ | $888 \pm 17$ |
| ParticleNet | 0.940 | 0.9858 | $397 \pm 7$ | $1615 \pm 93$ |
| JEDI-net (w/ $\sum O$) | 0.930 | 0.9807 | — | 774.6 |
| PCT | 0.940 | 0.9855 | $392 \pm 7$ | $1533 \pm 101$ |
| LGN | 0.929 | 0.964 | — | $435 \pm 95$ |
| rPCN | — | 0.9845 | $364 \pm 9$ | $1642 \pm 93$ |
| ParT | 0.940 | 0.9858 | $413 \pm 16$ | $1602 \pm 81$ |
| **ParT-f.t.** | **0.944** | **0.9877** | **691 ± 15** | **2766 ± 130** |

*Model complexity*

| | Accuracy | # params | FLOPs |
|---|---|---|---|
| PFN | 0.772 | 86.1 k | 4.62 M |
| P-CNN | 0.809 | 354 k | 15.5 M |
| ParticleNet | 0.844 | 370 k | 540 M |
| **ParT** | **0.861** | 2.14 M | 340 M |
| ParT (plain) | 0.849 | 2.13 M | 260 M |

***Significant performance improvement.***
***Similar computational cost.***

# Summary & Outlook

# A charming journey

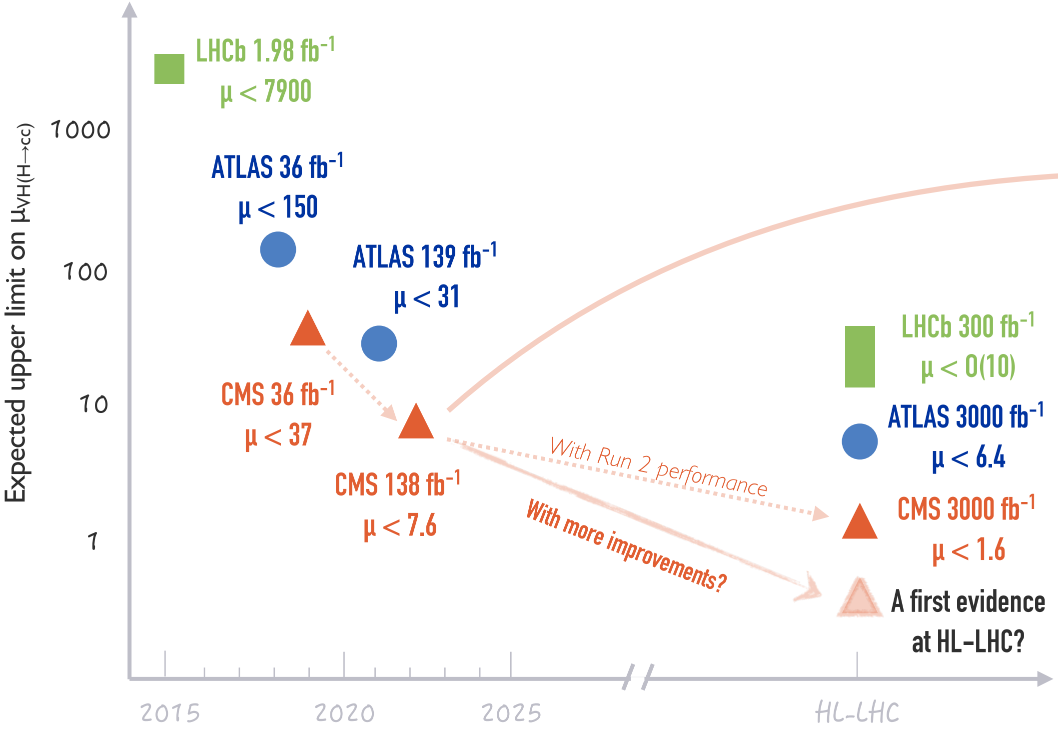


From $\mathcal{O}(1000)$ to $\mathcal{O}(100)$ to $\mathcal{O}(10)$ in ~5 years.
*A combined effort and creativity from instrumentation, physics objects and analysis techniques!*

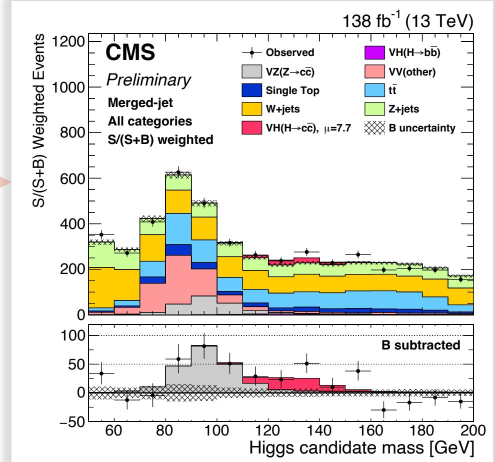


*First observation of Z → cc at a hadron collider!*
*Opening a new era for future explorations.*

- More channels: ttH(cc), VBF H(cc), indirect constraints, etc.
- Improvements in advanced analysis techniques (e.g., Deep Learning) and instrumentation (e.g., tracker)
- Reduction of systematic uncertainties: c-tagging, event modeling, theoretical uncertainties, …

*A charming journey ahead!*

# Backups

# H → cc searches at the LHC



- ATLAS:
  - [Phys. Rev. Lett. 120 (2018) 211802] (36 $fb^{-1}$)
  - [arXiv:2201.11428] (139 $fb^{-1}$)
  - [ATL-PHYS-PUB-2021-039] (HL-LHC projection, 3000 $fb^{-1}$)
- CMS:
  - [JHEP 03 (2020) 131] (36 $fb^{-1}$)
  - [CMS-PAS-HIG-21-008] (138 $fb^{-1}$; HL-LHC projection, 3000 $fb^{-1}$)
- LHCb:
  - [LHCb-CONF-2016-006] (1.98 $fb^{-1}$)
  - [LHCb-PUB-2018-009] (HL-LHC projection, 300 $fb^{-1}$)

# Higgs-charm coupling at HL-LHC

- Expected sensitivity at HL-LHC [CERN-2019-007]

| | |
|---|---|
| $H \rightarrow cc$ decay | $\|\kappa_c\| <$ ~1-2 |
| cH production | $\|\kappa_c\| <$ ~2-3 |
| $H \rightarrow J/\Psi\gamma$ | $\|\kappa_c\| <$ ~80 |
| $p_T(H)$ distribution | $\|\kappa_c\| <$ ~10 |
| WH charge assymetry | $\|\kappa_c\| <$ ~4-5 |

# ATLAS HL-LHC projection for H → cc

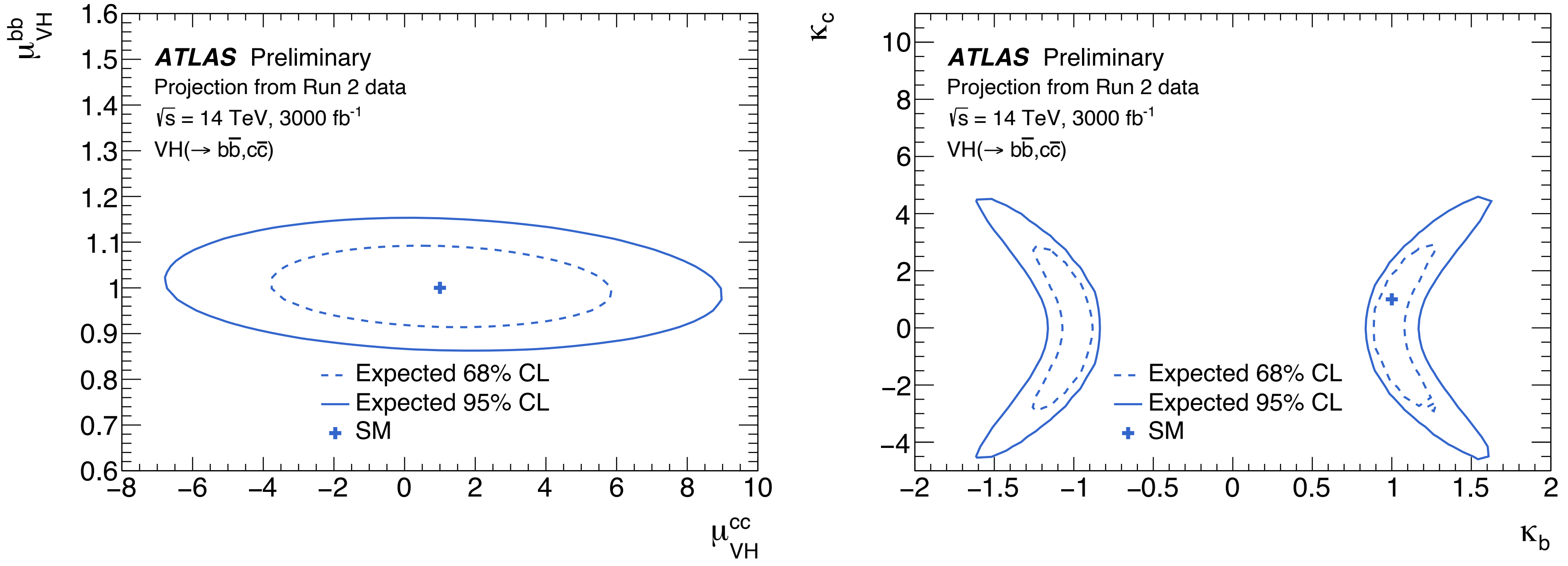

# Baseline event selections



## Merged-jet topology

| Variable | 0L | 1L | 2L |
|---|---|---|---|
| $p_T^\ell$ | — | (>25,>30) | >20 |
| Lepton isolation | — | (<0.06, —) | (<0.25, —) |
| $N_{a\ell}$ | =0 | =0 | — |
| $M(\ell\ell)$ | — | — | 75–105 |
| $N_{small\text{-}R}^{aj}$ | <2 | <2 | <3 |
| $p_T^{miss}$ | >200 | >60 | — |
| $p_T(V)$ | >200 | >150 | >150 |
| $p_T(H_{cand})$ | >300 | >300 | >300 |
| $m\ (H_{cand})$ | 50–200 | 50–200 | 50–200 |
| $\Delta\phi(V, H_{cand})$ | >2.5 | >2.5 | >2.5 |
| $\Delta\phi(\vec{p}_T^{miss}, j)$ | >0.5 | — | — |
| $\Delta\phi(\vec{p}_T^{miss}, \ell)$ | — | <1.5 | — |
| Kinematic BDT | >0.55 | 0.55–0.7, >0.7 | >0.55 |
| $c\bar{c}$ discriminant | | | |
| High purity | >0.99 | >0.99 | >0.99 |
| Medium purity | 0.96–0.99 | 0.96–0.99 | 0.96–0.99 |
| Low purity | 0.90–0.96 | 0.90–0.96 | 0.90–0.96 |

## Resolved-jet topology

| Variable | 0L | 1L | 2L low-$p_T(V)$ | 2L high-$p_T(V)$ |
|---|---|---|---|---|
| $p_T^\ell$ | — | (>25,>30) | >20 | >20 |
| Lepton isolation | — | (<0.06, —) | (<0.25, —) | (<0.25, —) |
| $N_{a\ell}$ | =0 | =0 | — | — |
| $M(\ell\ell)$ | — | — | 75–105 | 75–105 |
| $p_T(j_1)$ | >60 | >25 | >20 | >20 |
| $p_T(j_2)$ | >35 | >25 | >20 | >20 |
| $CvsL(j_1)$ | >0.225 | >0.225 | >0.225 | >0.225 |
| $CvsB(j_2)$ | >0.4 | >0.4 | >0.4 | >0.4 |
| $N_{small\text{-}R}^{aj}$ | — | <2 | — | — |
| $p_T^{miss}$ | > 170 | — | — | — |
| $p_T^{miss}$ significance | — | >4 | — | — |
| $p_T(V)$ | >170 | >100 | 60–150 | >150 |
| $p_T(H_{cand})$ | >120 | >100 | — | — |
| $m\ (H_{cand})$ | <250 | <250 | <250 | <250 |
| $\Delta\phi(V, H_{cand})$ | >2.0 | >2.5 | >2.5 | >2.5 |
| $\Delta\phi(\vec{p}_T^{miss}, j)$ | >0.5 | — | — | — |
| $\Delta\phi(\vec{p}_T^{miss}, \ell)$ | — | <2.0 | — | — |

# Uncertainties

- Breakdown of the uncertainties in each topology



**Merged-jet topology**

Table 3: The relative contributions to the total uncertainty on $\mu_{VH(H\to c\bar{c})}$ in the merged-jet analysis, with a best fit value $\mu_{VH(H\to c\bar{c})} = 8.7^{+4.6}_{-4.0}$.

| Uncertainty source | $\Delta\mu / (\Delta\mu)_{tot}$ |
|---|---|
| **Statistical** | **88%** |
| Background normalizations | 39% |
| **Experimental** | **40%** |
| Sizes of the simulated samples | 24% |
| Charm identification efficiencies | 26% |
| Jet energy scale and resolution | 15% |
| Simulation modeling | 1% |
| Luminosity | 5% |
| Lepton identification efficiencies | 2% |
| **Theory** | **25%** |
| Backgrounds | 21% |
| Signal | 14% |

**Resolved-jet topology**

Table 4: The relative contributions to the total uncertainty on $\mu_{VH(H\to c\bar{c})}$ in the resolved-jet analysis, with a best fit value $\mu_{VH(H\to c\bar{c})} = -9.5 \pm 9.6$.

| Uncertainty source | $\Delta\mu / (\Delta\mu)_{tot}$ |
|---|---|
| **Statistical** | **66%** |
| Background normalizations | 28% |
| **Experimental** | **72%** |
| Sizes of the simulated samples | 59% |
| Charm identification efficiencies | 27% |
| Jet energy scale and resolution | 17% |
| Simulation modeling | 20% |
| Luminosity | 13% |
| Lepton identification efficiencies | 10% |
| **Theory** | **22%** |
| Backgrounds | 21% |
| Signal | 7% |

# BDT input variables: Merged-jet topology

| Variable | Description | 0-lepton | 1-lepton | 2-lepton |
|---|---|---|---|---|
| $p_{\mathrm{T}}(\mathrm{V})$ | vector boson transverse momentum | ✓ | ✓ | ✓ |
| $\Delta R(\ell,\ell)$ | angular separation between the two leptons | — | — | ✓ |
| $p_{\mathrm{T}}\ (\mathrm{H}_{\mathrm{cand}})$ | $\mathrm{H}_{\mathrm{cand}}$ transverse momentum | ✓ | ✓ | ✓ |
| $\lvert\eta(\mathrm{H}_{\mathrm{cand}})\rvert$ | absolute value of the $\mathrm{H}_{\mathrm{cand}}$ pseudorapidity | ✓ | — | — |
| $\Delta\phi(\mathrm{V},\mathrm{H}_{\mathrm{cand}})$ | azimuthal angle between vector boson and $\mathrm{H}_{\mathrm{cand}}$ | ✓ | ✓ | ✓ |
| $p_{\mathrm{T}}^{\mathrm{miss}}$ | missing transverse momentum | — | ✓ | — |
| $\Delta\eta(\mathrm{H}_{\mathrm{cand}},\ell)$ | difference in pseudorapidity between $\mathrm{H}_{\mathrm{cand}}$ and the lepton | — | ✓ | — |
| $\Delta\eta(\mathrm{H}_{\mathrm{cand}},\,)$ | difference in pseudorapidity between $\mathrm{H}_{\mathrm{cand}}$ and vector boson | — | — | ✓ |
| $\Delta\eta(\mathrm{H}_{\mathrm{cand}},\mathrm{j})$ | min. difference in pseudorapidity between $\mathrm{H}_{\mathrm{cand}}$ and small-$R$ jets | ✓ | ✓ | ✓ |
| $\Delta\eta(\ell,\mathrm{j})$ | min. difference in pseudorapidity between the lepton and small-$R$ jets | — | ✓ | — |
| $\Delta\eta(\mathrm{V},\mathrm{j})$ | min. difference in pseudorapidity between vector boson and small-$R$ jets | — | — | ✓ |
| $\Delta\phi(\vec{p}_{\mathrm{T}}^{\mathrm{miss}},\mathrm{j})$ | azimuthal angle between $\vec{p}_{\mathrm{T}}^{\mathrm{miss}}$ and closest small-$R$ jet | ✓ | — | — |
| $\Delta\phi(\vec{p}_{\mathrm{T}}^{\mathrm{miss}},\ell)$ | azimuthal angle between $\vec{p}_{\mathrm{T}}^{\mathrm{miss}}$ and lepton | — | ✓ | — |
| $m_{\mathrm{T}}$ | transverse mass of lepton $\vec{p}_{\mathrm{T}} + \vec{p}_{\mathrm{T}}^{\mathrm{miss}}$ | — | ✓ | — |
| $N_{\mathrm{small}\text{-}R}^{\mathrm{aj}}$ | number of additional small-$R$ jets | ✓ | ✓ | ✓ |

# BDT input variables: Resolved-jet topology

| Variable | Description | 0-lepton | 1-lepton | 2-lepton |
|---|---|---|---|---|
| $m\,(\mathrm{H_{cand}})$ | $\mathrm{H_{cand}}$ mass | ✓ | ✓ | ✓ |
| $p_{\mathrm{T}}\,(\mathrm{H_{cand}})$ | $\mathrm{H_{cand}}$ transverse momentum | — | ✓ | ✓ |
| $p_{\mathrm{T}}(\mathrm{V})$ | vector boson transverse momentum | — | ✓ | ✓ |
| $m_{\mathrm{T}}(\mathrm{V})$ | vector boson transverse mass | — | ✓ | — |
| $p_{\mathrm{T}}^{\mathrm{miss}}$ | missing transverse momentum | ✓ | ✓ | — |
| $p_{\mathrm{T}}(\mathrm{V})/p_{\mathrm{T}}(\mathrm{H_{cand}})$ | ratio between vector boson and H transverse momenta | ✓ | ✓ | ✓ |
| $CvsL_{\mathrm{max}}$ | *CvsL* value of the leading *CvsL* jet | ✓ | ✓ | ✓ |
| $CvsB_{\mathrm{max}}$ | *CvsB* value of the leading *CvsL* jet | ✓ | ✓ | ✓ |
| $CvsL_{\mathrm{min}}$ | *CvsL* value of the subleading *CvsL* jet | ✓ | ✓ | ✓ |
| $CvsB_{\mathrm{min}}$ | *CvsB* value of the subleading *CvsL* jet | ✓ | ✓ | ✓ |
| $p_{\mathrm{Tmax}}$ | $p_{\mathrm{T}}$ of the leading *CvsL* jet | ✓ | ✓ | ✓ |
| $p_{\mathrm{Tmin}}$ | $p_{\mathrm{T}}$ of the subleading *CvsL* jet | ✓ | ✓ | ✓ |
| $\Delta\phi(\mathrm{V},\mathrm{H_{cand}})$ | azimuthal angle between vector boson and H | ✓ | ✓ | ✓ |
| $\Delta R(\mathrm{j_1},\mathrm{j_2})$ | $\Delta R$ between leading and subleading *CvsL* jets | — | ✓ | ✓ |
| $\Delta\phi(\mathrm{j_1},\mathrm{j_2})$ | azimuthal angle between leading and subleading *CvsL* jets | ✓ | ✓ | — |
| $\Delta\eta(\mathrm{j_1},\mathrm{j_2})$ | difference in pseudorapidity between leading and subleading *CvsL* jets | ✓ | ✓ | ✓ |
| $\Delta\phi(\ell_1,\ell_2)$ | azimuthal angle between leading and subleading $p_{\mathrm{T}}$ leptons | — | — | ✓ |
| $\Delta\eta(\ell_1,\ell_2)$ | difference in pseudorapidity between leading and subleading $p_{\mathrm{T}}$ leptons | — | — | ✓ |
| $\Delta\phi(\ell_1,\mathrm{j_1})$ | azimuthal angle between leading $p_{\mathrm{T}}$ lepton and leading *CvsL* jet | — | ✓ | — |
| $\Delta\phi(\ell_2,\mathrm{j_1})$ | azimuthal angle between subleading $p_{\mathrm{T}}$ lepton and leading *CvsL* jet | — | — | ✓ |
| $\Delta\phi(\ell_2,\mathrm{j_2})$ | azimuthal angle between subleading $p_{\mathrm{T}}$ lepton and subleading *CvsL* jet | — | — | ✓ |
| $\Delta\phi(\ell_1,p_{\mathrm{T}}^{\mathrm{miss}})$ | azimuthal angle between leading $p_{\mathrm{T}}$ lepton and missing transverse momentum | — | ✓ | — |
| $\Delta\eta(\ell_1,\mathrm{b})$ | difference in pseudorapidity between leading $p_{\mathrm{T}}$ lepton and b-tagged jet from top quark decay | — | ✓ | — |
| $\Delta\phi(\ell_1,\mathrm{b})$ | azimuthal angle between leading $p_{\mathrm{T}}$ lepton and b-tagged jet from top quark decay | — | ✓ | — |
| $\Delta R(\ell_1,\mathrm{b})$ | $\Delta R$ between leading $p_{\mathrm{T}}$ lepton and b-tagged jet from top quark decay | — | ✓ | — |
| $CvsL_{\mathrm{b}}$ | *CvsL* value of the b-tagged jet from top quark decay | — | ✓ | — |
| $CvsB_{\mathrm{b}}$ | *CvsB* value of the b-tagged jet from top quark decay | — | ✓ | — |
| $P(b{+}bb)_{\mathrm{b}}$ | *DeepJet prob(b+bb)* value of the b-tagged jet from top quark decay | — | ✓ | — |
| $m(\mathrm{t})$ | Reconstructed top quark mass | — | ✓ | — |
| $N_{\mathrm{small}\text{-}R}^{\mathrm{aj}}$ | Number of small-*R* additional jets after the FSR subtraction | — | ✓ | — |
| $\sigma_{cReg}(\mathrm{j_1})$ | leading $p_{\mathrm{T}}$ jet resolution from c-jet energy regression | ✓ | ✓ | ✓ |
| $\sigma_{cReg}(\mathrm{j_2})$ | subleading $p_{\mathrm{T}}$ jet resolution from c-jet energy regression | ✓ | ✓ | ✓ |
| $\Delta\eta(\mathrm{V},\mathrm{H_{cand}})\|_{\mathrm{kinfit}}$ | difference in pseudorapidity between vector boson and $\mathrm{H_{cand}}$, after kinematic-fit | — | — | ✓ |
| $\Delta\phi(\mathrm{V},\mathrm{H_{cand}})\|_{\mathrm{kinfit}}$ | azimuthal angle between vector boson and $\mathrm{H_{cand}}$, after kinematic-fit | — | — | ✓ |
| $m(\mathrm{H_{cand}})\|_{\mathrm{kinfit}}$ | $\mathrm{H_{cand}}$ mass after kinematic-fit | — | — | ✓ |
| $p_{\mathrm{T}}(\mathrm{H_{cand}})\|_{\mathrm{kinfit}}$ | $\mathrm{H_{cand}}$ transverse momentum after kinematic-fit | — | — | ✓ |
| $p_{\mathrm{Tmax}}\|_{\mathrm{kinfit}}$ | $p_{\mathrm{T}}$ of the leading *CvsL* jet after kinematic-fit | — | — | ✓ |
| $p_{\mathrm{Tmin}}\|_{\mathrm{kinfit}}$ | $p_{\mathrm{T}}$ of the subleading *CvsL* jet after kinematic-fit | — | — | ✓ |
| $p_{\mathrm{T}}(\mathrm{V})/p_{\mathrm{T}}(\mathrm{H_{cand}})\|_{\mathrm{kinfit}}$ | ratio between vector boson and $\mathrm{H_{cand}}$ transverse momenta after kinematic-fit | — | — | ✓ |
| $\sigma(\mathrm{H_{cand}})\|_{\mathrm{kinfit}}$ | $\mathrm{H_{cand}}$ invariant mass resolution from kinematic fit | — | — | ✓ |

# Merged-jet topology: signal regions

2L(μμ), high cc-purity

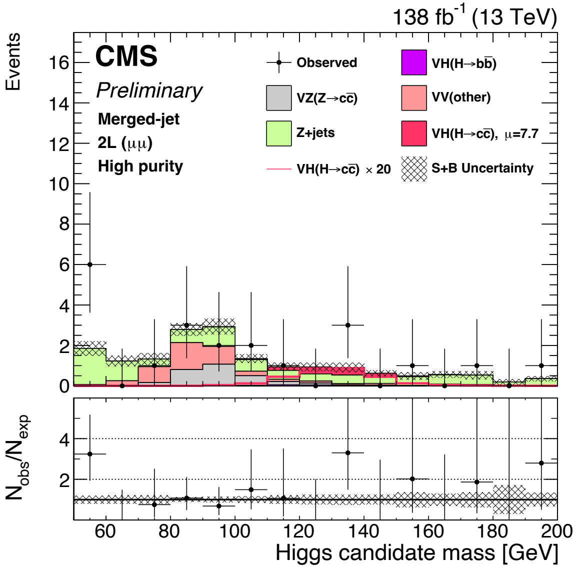


1L(e), high cc-purity

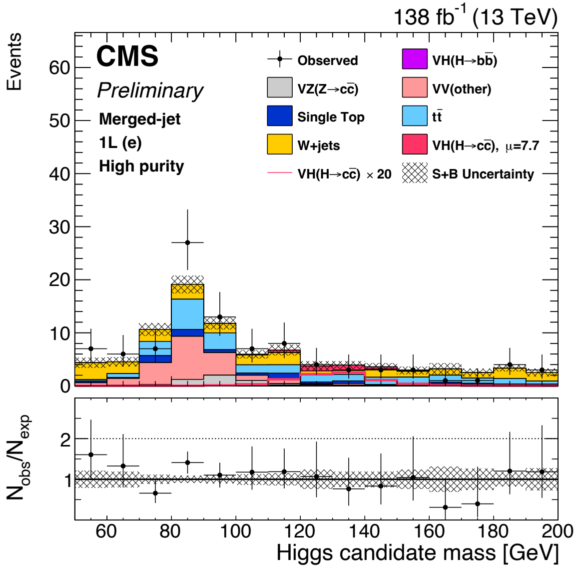


0L, high cc-purity

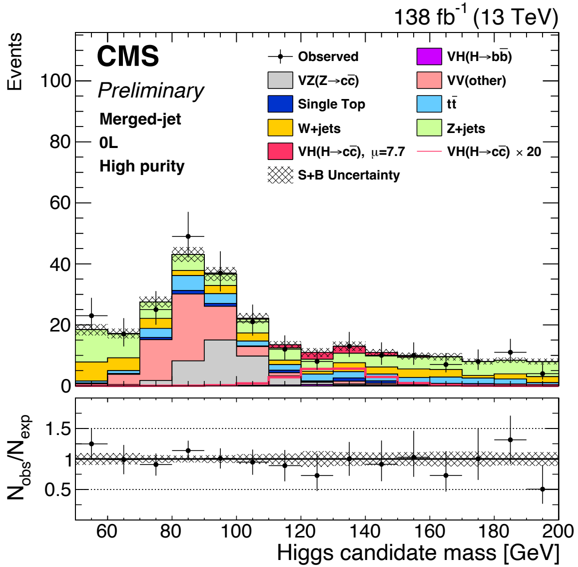

# Merged-jet topology: control regions



2L(ee), V+jets CR, low cc-purity

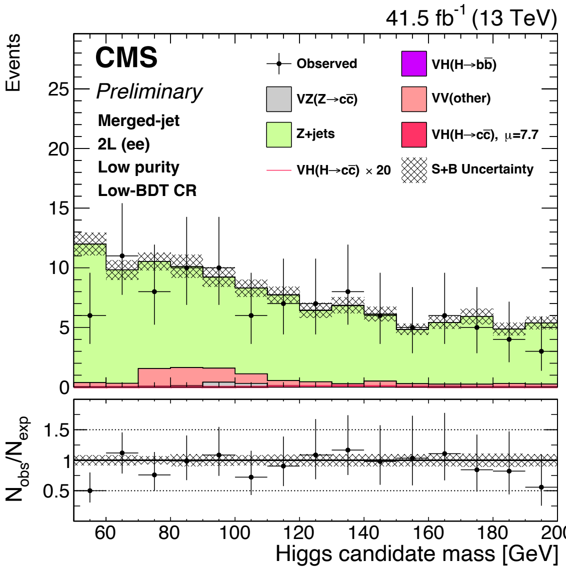


1L(μ), tt CR, high cc-purity

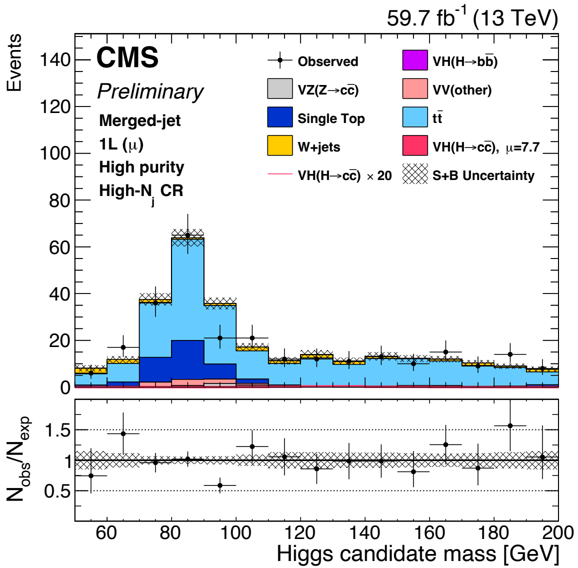


0L, V+jets CR, medium cc-purity

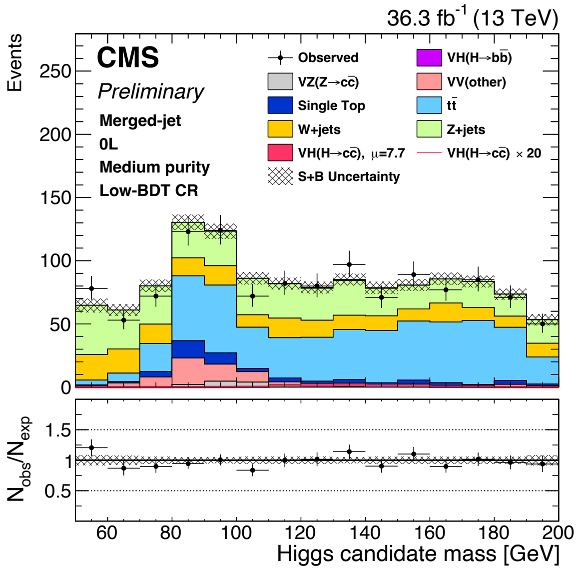

# Comparison of mass decorrelation methods



## DeepAK8-MD

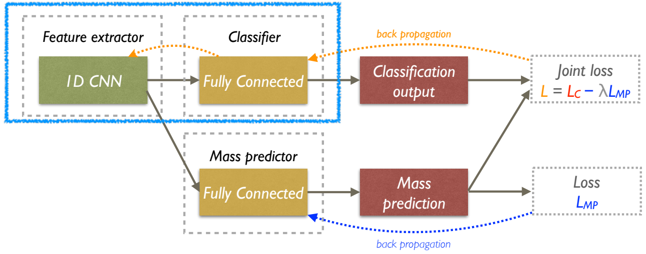


### Background jet mass

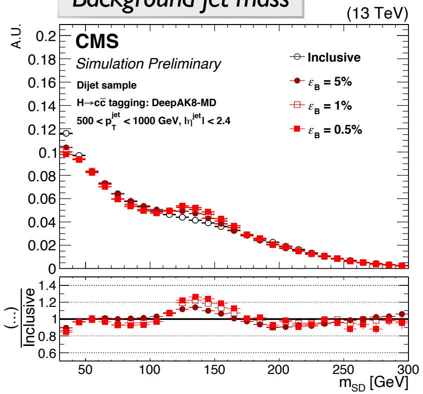


## ParticleNet-MD

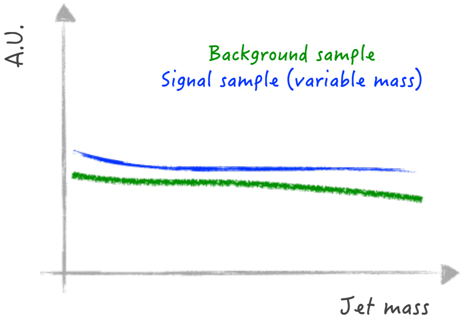


### Background jet mass

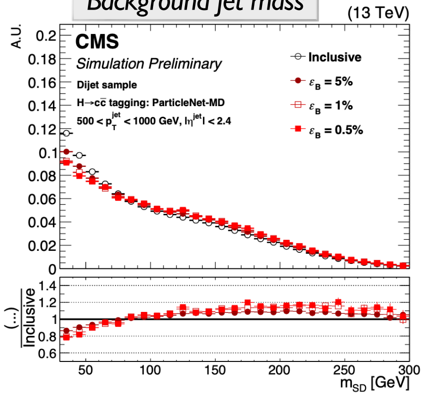


## H→cc tagging performance

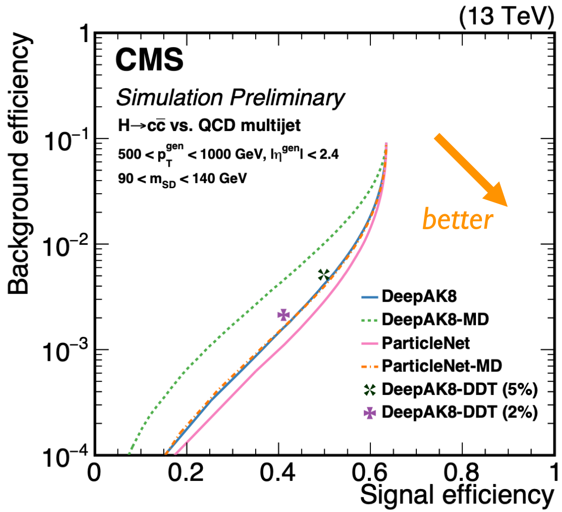

# Large-R jet mass regression

*Loss function: LogCosh*

$$L(y, y^p) = \sum_{i=1}^{n} \log(\cosh(y_i^p - y_i))$$

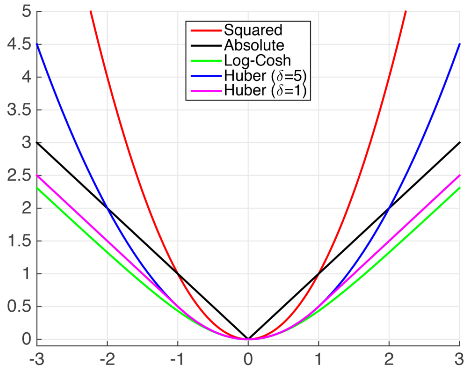


https://www.cs.cornell.edu/courses/cs4780/2015fa/web/lecturenotes/lecturenote10.html

*Signal jet mass resolution*

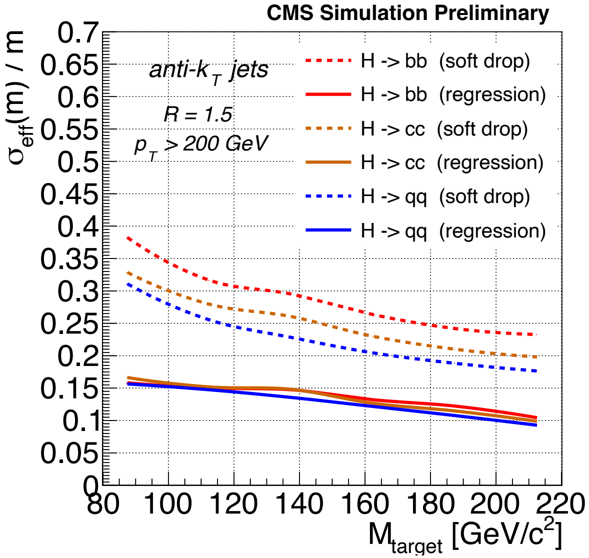


*Background jet mass response*

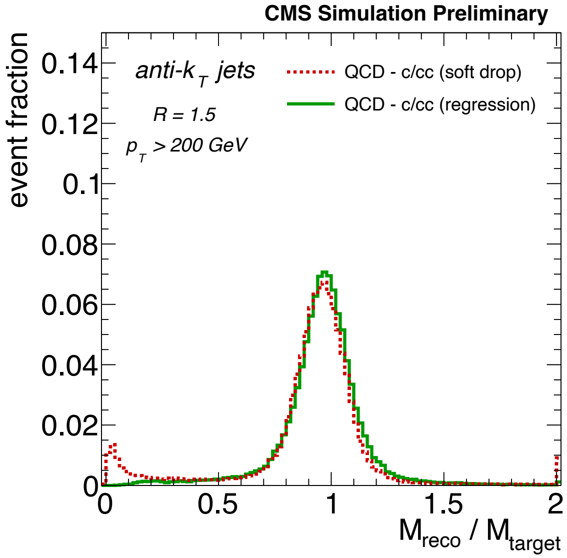

# Calibration of the cc-tagger

[CMS-DP-2022-005](#)



## Passing category

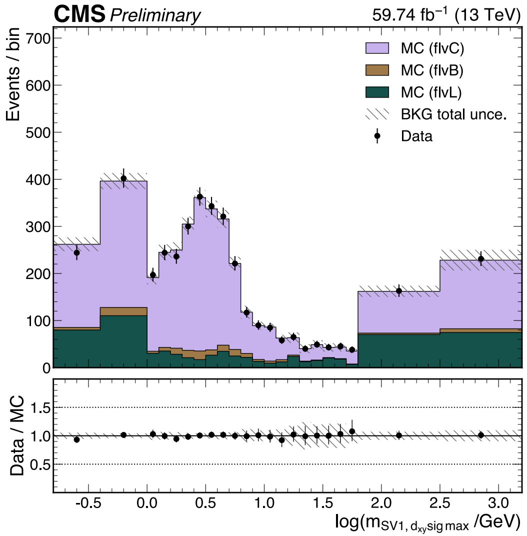


## Failing category

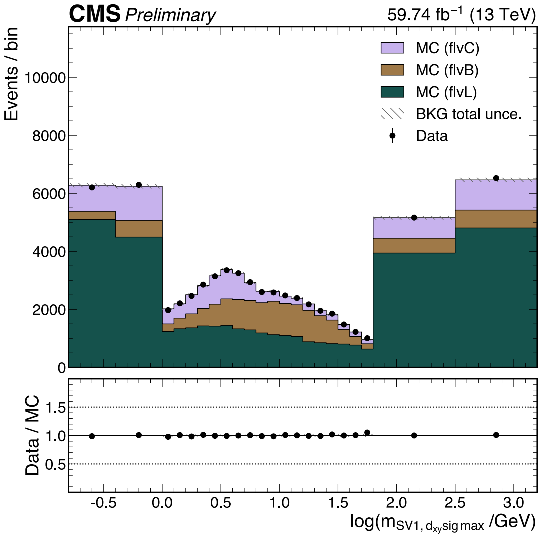


## cc-tagging scale factors

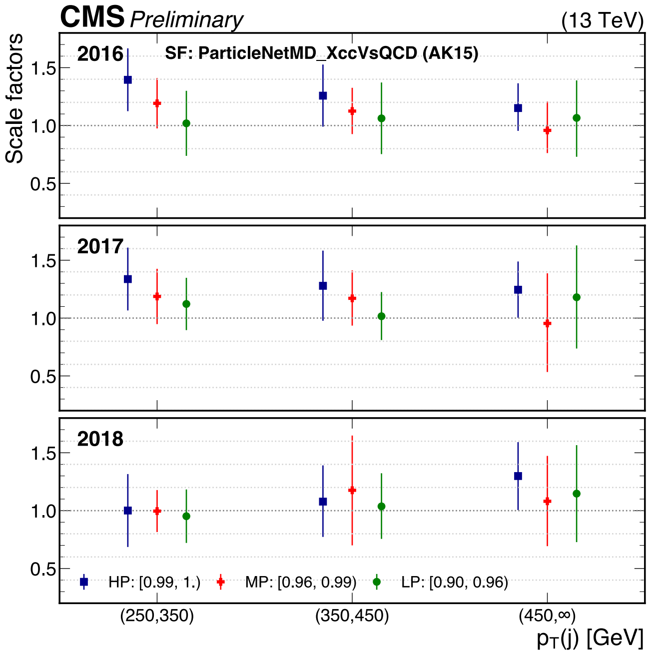

# C-tagger ROC curves

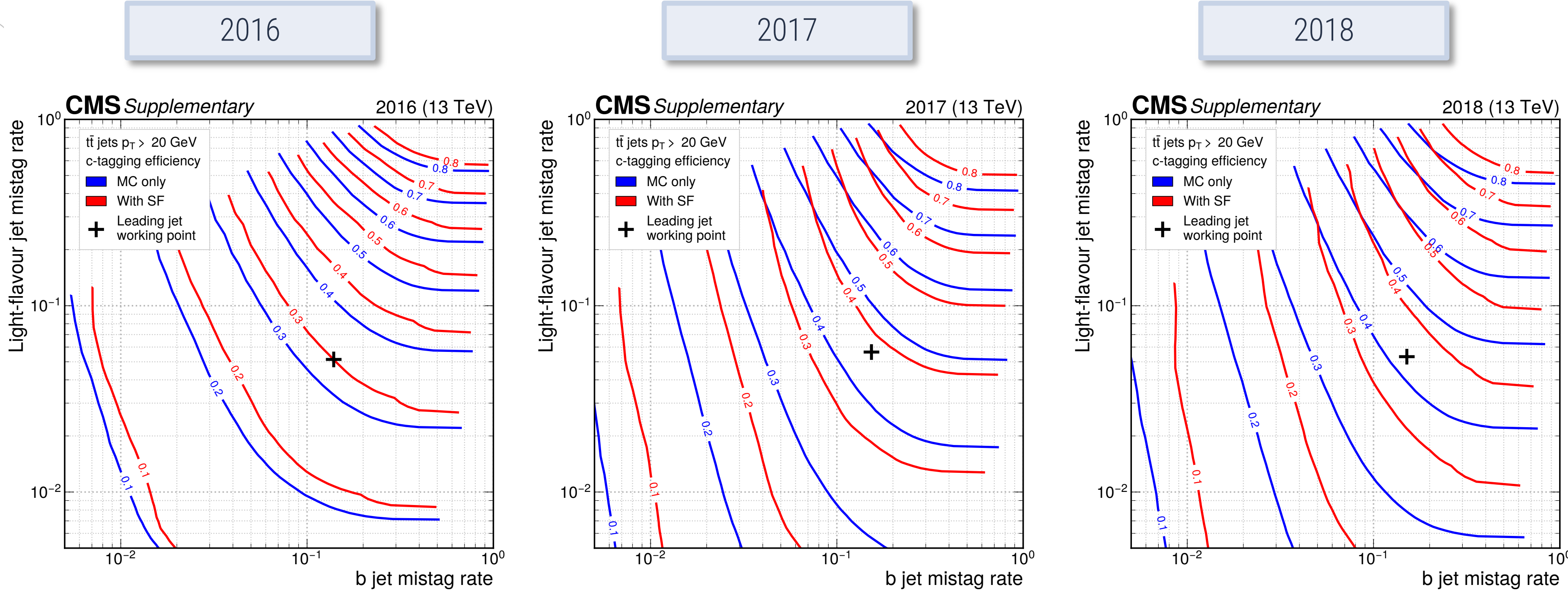


- CMS c-tagging WP: ~40% (c), ~16% (b), ~4% (light)
- ATLAS c-tagging WP [arXiv:2201.11428]: 27% (c), 8% (b), 1.6% (light)

# Transformer 101

Vaswani, Shazeer, Parmar, Uszkoreit, Jones, Gomez, Kaiser, Polosukhin, arXiv:1706.03762

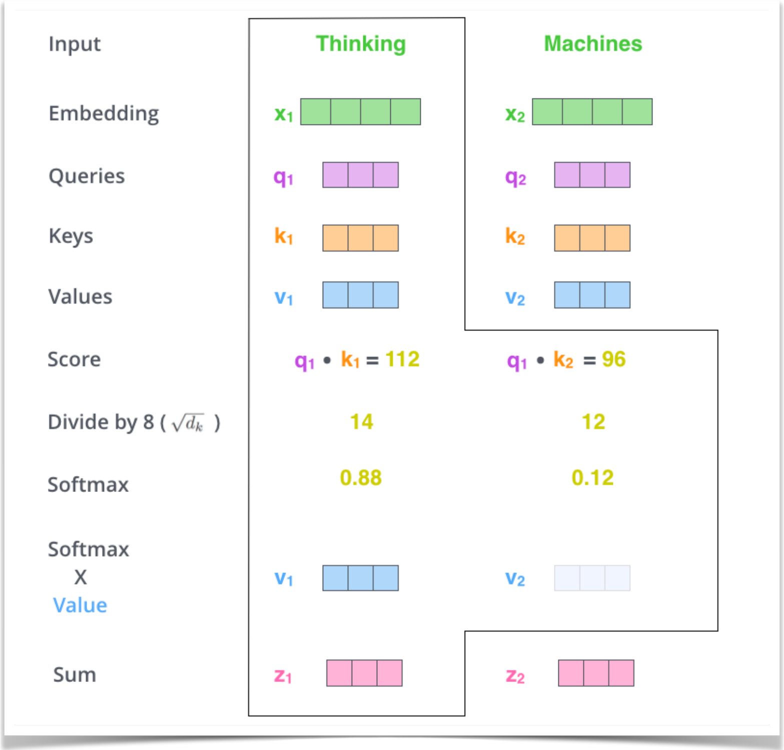


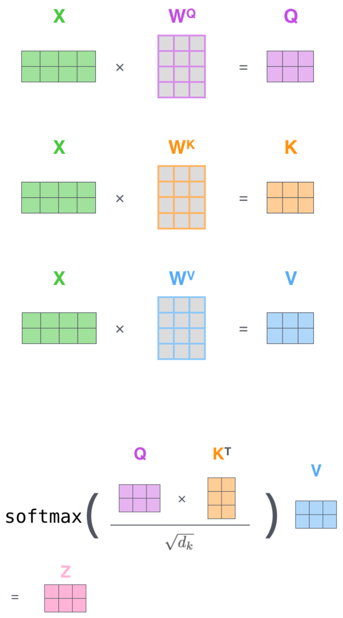


https://jalammar.github.io/illustrated-transformer/ X